



Empowered lives.
Resilient nations.

“National Adaptation Plan (NAP) to advance medium and long-term adaptation planning in Armenia”

UNDP-GCF/00104267 Project

Harmonization of Datasets and Scenarios used for Water Vulnerability Assessment due to Climate Change,
Preparation of Vulnerability Map, and
Delivery of Recommendations on Application of Remote Sensing Data for Water Vulnerability Assessment

Prepared by: Aleksandr Arakelyan, National Expert on Water Resources Climate Risk and Vulnerability Assessment



Yerevan, Armenia

November 2020

Contents

List of Tables.....	2
List of Figures.....	2
Background	3
1. Inventory and harmonization of models, algorithms, scenarios, and data sets used for currently available water resources vulnerability assessments in Armenia within the climate change context.....	4
<i>Introduction.....</i>	4
1.1 Scenarios	4
1.2 Climate Models.....	6
1.3 Climate Change Scenarios and Models used in Armenia.....	7
1.4 Algorithms and Models used for Water Resources Vulnerability Assessments in Armenia	8
1.5 Development of Water Resources Vulnerability Map for Armenia.....	15
2. Specific recommendations on tools, algorithms and remote sensing data to be applied for water resources vulnerability assessment in Armenia and preparation of vulnerability map of water resources due to climate change.....	22
2.1 Remote Sensing in Climate Change Studies.....	22
2.2 Basics of Water Resources Vulnerability Assessment: Hydrologic Cycle and Water Balance Models.....	22
2.3 Satellite Measurement of Precipitation.....	29
2.4 Satellite Measurement of Evapotranspiration	40
2.5 Land Surface Temperature (LST)	43
2.6 Land Use / Land Cover (LULC).....	44
2.7 Leaf Area Index (LAI)	45
2.8 Elevation.....	46
Next Steps	48
Literature.....	49

List of Tables

Table 1. Climate Change Scenarios Used in in Armenia.....	7
Table 2. Projected Changes of the Flow of Main Rivers in Armenia (IPCC RCP8.5 Scenario, METRAS Model) 16	16
Table 3. Projected Changes of the Surface Natural Flow in the Watershed Area of Ararat Valley under the IPCC RCP8.5 Scenario (IPCC RCP8.5 Scenario, METRAS Model)	18
Table 4. Projected Changes in Annual Surface Natural Flow, % (IPCC RCP8.5 Scenario, METRAS Model) .	19
Table 5. Projected Changes in Annual Surface Natural Flow, % (IPCC RCP8.5 Scenario, METRAS Model) .	19
Table 6. Vulnerability of Water Resources in Armenia due to the Climate Change (IPCC RCP8.5 Scenario, METRAS Model)	20

List of Figures

Figure 1. Observed Historic Emissions Compares with the Various IPCC SRES Scenarios.....	5
Figure 2. RCP Carbon Dioxide Emission Scenarios. Source: Mann & Kump, Dire Predictions: Understanding Climate Change, 2nd Edition © 2015 Dorling Kindersley Limited.....	6
Figure 3. Import of Hydro-Meteorological Time Series Data from Excel Sheets to the GIS Layers	13
Figure 4. Decision Support System (DSS) Extension of ArcGIS	13
Figure 5. Historic Trends Component of DSS.....	14
Figure 6. Projections Component of DSS	14
Figure 7. Example of the Output of Projections Component of DSS	15
Figure 8. Water Resources Vulnerability due to Climate Change, IPCC RCP8.5 Scenario, METRAS Model ..	21
Figure 9. The Global Water Cycle. Source: Technical University of Wien.....	23
Figure 10. Elements of the Global Water Cycle. Source: Jones, 1997.....	24
Figure 11. A Simple Representation of Water Balance Model. Source: Technical University of Wien	25
Figure 12. SWAT Model Inputs and Output (Shivhare et al., 2018)	26
Figure 13. Model flowchart that illustrates the integration of the Soil and Water Assessment Tool (SWAT) and Water Evaluation and Planning (WEAP) models.....	26
Figure 14. The Global Observing System of the Water Cycle	27
Figure 15. Meteorological Satellite Network	29
Figure 16. Evolution of the satellite constellation for precipitation measurements	29
Figure 17. Comparison of monthly Cold Cloud Duration map of Africa (left) with long term mean of precipitation interpolated from raingauges (right).....	31
Figure 18. Global rain rate in mm/h derived from AMSR2, a passive microwave radiometer on board of JAXA's GCOM W1 satellite (https://disc.gsfc.nasa.gov)	31
Figure 19. TMI: Passive microwave sensor that measures in five frequencies: 10.7 (45 km spatial resolution), 19.4, 21.3, 37, and 85.5 GHz (5 km spatial resolution). Swath width 780 km.....	32
Figure 20. Daily Accumulated Precipitation (combined microwave-IR) estimate (mm), TMPA.....	33
Figure 21. Satellite Estimated Precipitation (mm), CMORPH.....	34
Figure 22. Estimating Rainfall from Satellite Soil Moisture Data	35
Figure 23. Daily Mean Temperature Calculated from the Different Satellite Products. Source: Technical University of Wien.....	36
Figure 24. Maximum 5-day precipitation amount Calculated from the Different Satellite Products. Source: Technical University of Wien	36
Figure 25. Spatial patterns of annual precipitation over Armenia for GPCC-V8 and CRU datasets	37
Figure 26. Long-term trends in precipitation over Armenia for GPCC-V8 and CRU datasets.....	38
Figure 27. Spatial patterns of annual precipitation over Armenia for GPCC-V8 (50km), CRU (50km) and PERSIANN-CDR (25km) datasets over the period (1983-2015).....	39
Figure 28. Precipitation trends over the three decades of study for the three datasets (GPCC-V8, CRU and PERSIANN-CDR) over Armenia for GPCC-V8 and CRU datasets.....	39
Figure 29. GLEAM Algorithm and Products	40
Figure 30. GLDAS_NOAH025_3H: GLDAS Noah Land Surface Model L4 3 hourly 0.25 x 0.25 degree V2.1 .	41
Figure 31. Global Annual Evapotranspiration (2000-2006) mm/yr, MOD16 Dataset	42
Figure 32. Land Surface Temperature composite for September 2016 of the Copernicus Sentinel-3 Satellite's SLSTR Instrument (Processed by D. Ghent, University of Southampton)	44
Figure 33. Land cover and land use classification performance of machine learning algorithms using Sentinel-2 data	44
Figure 34. Land cover / Land Use Map of Ararat Valley	45
Figure 35. Leaf Area Index (LAI) Products in Coprnicus Global Land Service Portal	46
Figure 36. SRTM DEM with 1 arc-second Resolution for the Territory of Armenia	47

Background

This report is prepared within the UNDP-GCF project “National Adaptation Plan (NAP) to Advance Medium- and Long-Term Planning in Armenia”, which builds on the national climate priorities, and supports the Government of Armenia to advance its medium and long-term adaptation planning. The Green Climate Fund resources are used to enable the government to integrate climate change related risks, coping strategies and opportunities into ongoing development planning and budgeting processes. With the development of a NAP process, Armenia will lay the groundwork for the systemic and iterative identification of medium- and long-term climate-induced risks, climate change adaptation priorities, and specific activities that promote climate adaptive and resilient growth in its key sectors, including **water**.

The objective of the assignment is to perform climate risk and vulnerability analysis for the water sector, which is one of the key steps in formulation of water sector adaptation plan for Armenia. Before preparing this report, the recent study “Stocktaking exercise to identify legal, institutional, vulnerability assessment and adaptation gaps and barriers in water resources management under climate change conditions” was conducted within the UNDP-GCF project. The specific assumption of the assignment is to set a pathway for development of goals and objectives for climate adaptation, and further development and prioritization of adaptation measures.

This report summarizes the following steps of the assignment:

- Inventory and harmonization of models, algorithms, scenarios, and data sets used for currently available water resources vulnerability assessments in Armenia within the climate change context;
- Preparation of specific recommendations on tools, algorithms and remote sensing data to be applied for water resources vulnerability assessment in Armenia within the climate change contract and preparation of vulnerability map of water resources due to climate change.

Following this a subsequent report will be prepared in December 2020 on remote-sensing based assessment of evapotranspiration and forecasted projections, which will estimate and assess the evapotranspiration for the entire territory of Armenia based on remote sensing (calibrated based on the actual measurements performed at key reference meteorological stations of Armenia), including the projections of evapotranspiration for 2040, 2070 and 2100.

1. Inventory and harmonization of models, algorithms, scenarios, and data sets used for currently available water resources vulnerability assessments in Armenia within the climate change context

Introduction

Since 1998, when the First National Communication of Armenia on the Climate Change was adopted, a number of studies were conducted in order to analyze the climate change trends, develop climate change projections and assess possible climate change impacts on different sectors. One of the key elements of climate change impact studies in Armenia is the assessment of vulnerability of water resources and development of adaptation measures. Major works on water resources vulnerability assessment have commenced since 2008.

These studies are summarized in the form of four National Communications to UNFCCC, presented in the reports of donor-funded projects, as well as included in the river basin management plans (RBMP) for Akhuryan, Ararat, Southern, Hrazdan, and Sevan River Basin Districts (RBDs), research papers, relevant reports prepared during the implementation of the similar projects of international donor organizations.

In this chapter, the scenarios, models, algorithms, data sets etc. used for water resources vulnerability assessments are presented in a way to make them comparable.

1.1 Scenarios

A climate scenario is a plausible representation of future climate that has been constructed for explicit use in investigating the potential impacts of anthropogenic climate change. Climate scenarios often make use of climate projections (descriptions of the modelled response of the climate system to scenarios of greenhouse gas and aerosol concentrations), by manipulating model outputs and combining them with observed climate data (Climate Change, 2001).

In the climate change assessment conducted under the UNFCCC, the scenarios developed by Intergovernmental Panel on Climate Change (IPCC) are used. IPCC is an intergovernmental body of the United Nations that is dedicated to providing the world with objective, scientific information relevant to understanding the scientific basis of the risk of human-induced climate change, its natural, political, and economic impacts and risks, and possible response options.

The first group of 40 scenarios developed by International Panel on Climate Change (IPCC) in 2000 is presented in **Special Report on Emissions Scenarios (SRES)**. Each scenario is divided into one of four "families" (A1, A2, B1, B2), each with common themes (e.g: Population changes, energy sources, economic development, etc.) (Figure 1). In the case of the A1 model, there are 4 scenario "groups" based on the possibility of a certain energy source becoming more dominant (e.g: A1C scenarios are based on a coal-driven society). SRES use a sequential approach to determine their scenarios (Fourth Assessment Report, 2007). Political or legislative actions have no effect on the development of these scenarios. The scenarios are based on socio-economic futures; this setup requires each individual scenario (emission scenario, radiative forcing scenario, climate model scenario) to be formed in sequence with the previous scenario. If there is a change in any previous scenario, the whole sequence must be restarted. This makes the sequential approach time-consuming.

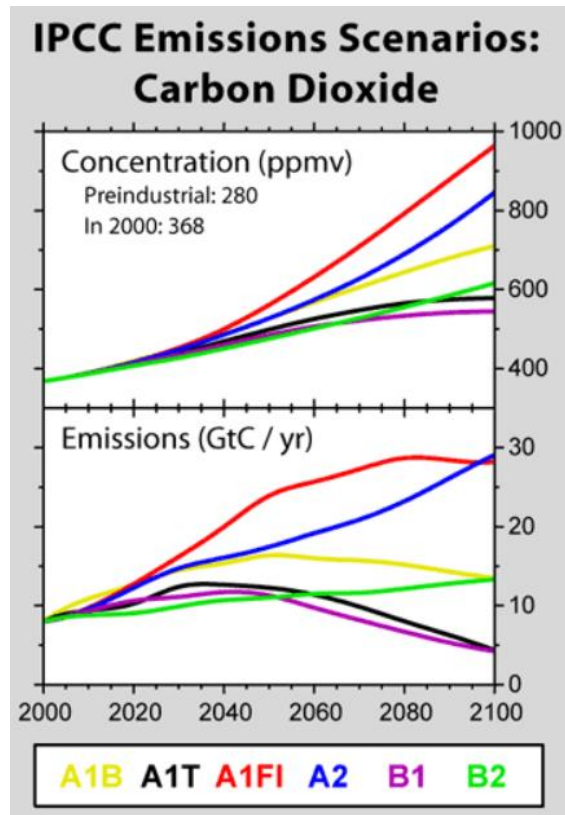


Figure 1. Observed Historic Emissions Compares with the Various IPCC SRES Scenarios.
Source: Robert A. Rohde: *Global Warming Art*

Representative Concentration Pathways (RCPs) are the group of 4 individual scenarios (RCP8.5, RCP6.0, RCP4.5, RCP2.6) developed by the IPCC in 2014 to supersede SRES (Figure 2). Each scenario consists of a specific radiative forcing projection and makes assumptions about future population, GDP, energy use, etc. based on the radiative forcing. RCPs use a parallel approach in the development of its scenarios. The parallel approach allows for policy changes to be implemented since the socio-economic scenarios are not the starting station for the RCPs. Scenarios are based off of radiative forcing projections; this allows for socio-economic, emissions and climate scenarios to be developed in parallel with each other. This way, changes can be made to one individual scenario without having to restart the whole sequence (<http://www.glisacclimate.org/node/2416>).

The RCPs cover a wider range than the scenarios from the Special Report on Emissions Scenarios (SRES) used in previous assessments, as they also represent scenarios with climate policy. In terms of overall forcing, RCP8.5 is broadly comparable to the SRES A2/A1FI scenario, RCP6.0 to B2 and RCP4.5 to B1. For RCP2.6, there is no equivalent scenario in SRES. As a result, the differences in the magnitude of AR4 and AR5 climate projections are largely due to the inclusion of the wider range of emissions assessed (Fifth Assessment Report, 2014).

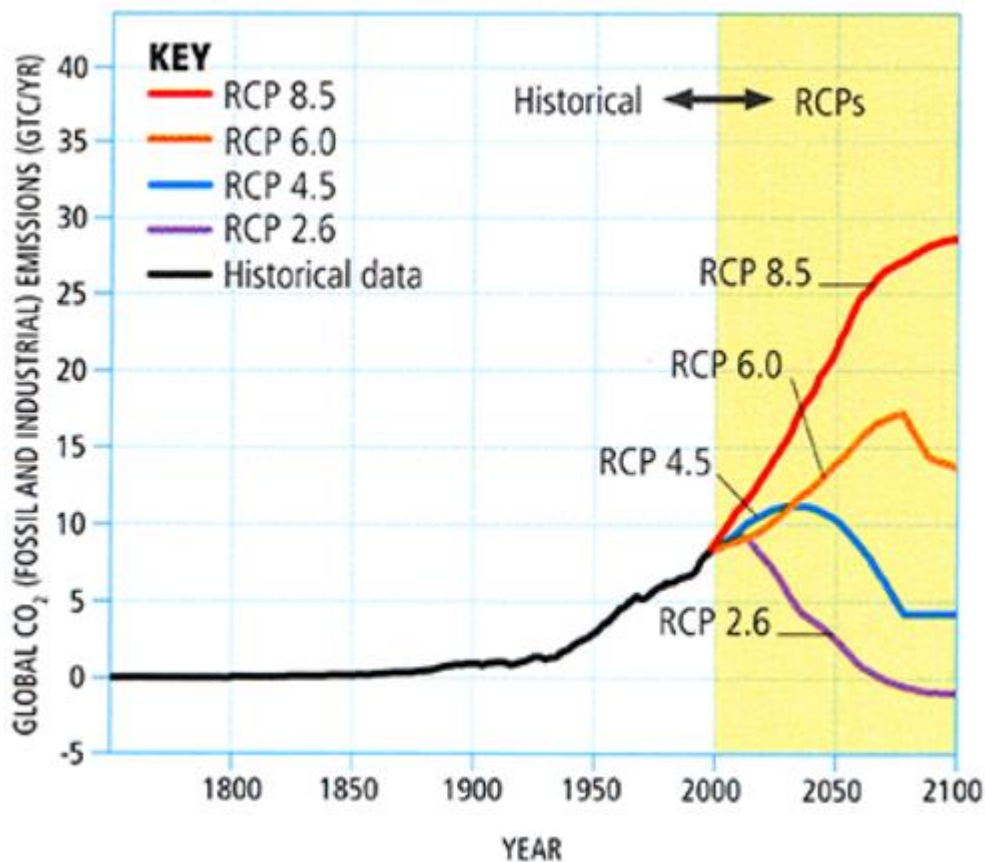


Figure 2. RCP Carbon Dioxide Emission Scenarios. Source: Mann & Kump, *Dire Predictions: Understanding Climate Change, 2nd Edition* © 2015 Dorling Kindersley Limited

1.2 Climate Models

Climate models are based on well-documented physical processes to simulate the transfer of energy and materials through the climate system. Climate models, also known as general circulation models or GCMs, use mathematical equations to characterize how energy and matter interact in different parts of the ocean, atmosphere, land. Building and running a climate model is complex process of identifying and quantifying Earth system processes, representing them with mathematical equations, setting variables to represent initial conditions and subsequent changes in climate forcing, and repeatedly solving the equations using powerful supercomputers.

General Circulation Models (GCMs), including Earth System Models (ESMs) that also simulate the carbon cycle are systematically upgrading, and the resolutions of regional climate model seem to become more reliable.

The PRECIS climate model (stands for "Providing Regional Climates for Impacts Studies"), used in the Second National Communication, is an atmospheric and land surface model of limited area and high resolution which is locatable over any part of the globe. Dynamical flow, the atmospheric sulphur cycle, clouds and precipitation, radiative processes, the land surface and the deep soil are all described. Boundary conditions are required at the limits of the model's domain to provide the meteorological forcing for the RCM.

In the recent studies on climate change in Armenia, CCSM4 and METRAS regional climate models were used.

Community Climate System Model 4.0 (CCSM4) developed by National Center for Atmospheric Research of America (NCAR) is the advanced model with four components: atmosphere, ocean, earth surface and glaciers, and has a 0.94° x 1.25° horizontal resolution (approximately 110 km) and 26 levels of elevation (up to 40 km).

The METRAS regional climate model has originally been developed at Meteorological Institute, University of Hamburg (Schlünzen, 1988, 1990). It is based on the results of ACCES, CNRM, MPIM, GFDL GCMs, Spatial resolution of the model is 12 km.

1.3 Climate Change Scenarios and Models used in Armenia

In the **First National Communication**, the observed and expected changes of the climatic characteristics of Armenia are estimated with the use of empirical-statistical methods, recommended by IPCC for that period and ArmStateHydromet hydrometeorological database, including the observations of 56 meteo stations for the period of 1885-1996. Climatic anomalies, i.e. the deviations of mean monthly, seasonal average meteorological parameters from their norms (mean values for 30-year period) are determined relative to WMO standard period of 1961-1990. Based on that, the increase of the air temperature by 2100 was estimated for 1.5 -2°C and reduction of atmospheric precipitation by 2100 was estimated for 10-15%.

In the **Second National Communication (2010)**, vulnerability of river flow due to the climate change was assessed using the values of climatic parameters for 2030, 2070, and 2100 projected IPCC SRES A2 scenario and trends in river flow and snow cover changes for 1991-2006.

In the Third National Communication (2015), Under the A2 scenario, the projected change in the aggregate volume of studied river flows in the territory of Armenia will decrease approximately by 11.9% by 2030, 24% by 2070, and 37.8% by 2100.

Fourth National Communication of Armenia to the UNFCCC is planned to finalize in 2020. The report on “The Vulnerability Assessment of Water Resources of the Republic of Armenia under the Climate Change” (2018) have been prepared within the scope of the project within the framework of the “Development of Armenia’s Fourth National Communication to the UNFCCC and Second Biennial Update Report” UNDP/GEF project. In that report, the assessments of climate change impacts conducted within the framework of the Third National Communication were reviewed and the correlations between climatic parameters and surface flow for each of the main river basins of Armenia were analyzed. After that, vulnerability assessment of the water resources of main river basins, reservoirs, and Lake Sevan were conducted using the physico-statistical or regression model based on the climate change projections obtained from CCSM4 and METRAS climate models for the periods of 2011-2040, 2041-2070, and 2071-2100.

The scenarios and models used in the National Communications have been also applied for water resources vulnerability assessments in other studies conducted in Armenia, including the development of basin management plans.

Table 1. Climate Change Scenarios Used in in Armenia

Scenario/Model	Projection period	Projected Temperature change, °C	Projected Precipitation change, %	NC / RBMP / Report	Territory, River Basin
Empiric scenario	up to 2100	+2	-10	First NC	Armenia
SRES A2 / MAGICC/SCENGEN	up to 2030	+1.1 – +1.2	-2 – -6	Second NC	Armenia
	2031-2070	+3.2 – +3.4	-6 – -17	Second NC	

	2071-2100	+5.3 – +5.7	-10 – -27	Second NC	
SRES A2 / PRECIS	up to 2030	+1	-3	Second NC	Armenia
	2031-2070	+3	-6	Second NC	
	2071-2100	+4	-9	Second NC	
SRES B1 / PRECIS	up to 2030	+0.7	+5	Southern BMP	Syunik Marz
	2031-2070	+1.4	+9	Southern BMP	Syunik Marz
	2071-2100	+2.4	+11	Southern BMP	Syunik Marz
SRES B2 / MAGICC/SCENGEN	up to 2030	+1.0 – +1.1	-2 – -6	Second NC	Armenia
	2031-2070	+2.9 – +3.0	-3 – -15	Second NC	
	2071-2100	+4.8 – +5.1	-8 – -24	Second NC	
RCP6.0 / CCSM4	up to 2040	+1.3	+5.3	Third NC; Fourth NC	Armenia
	2041-2070	+2.6	+5.8	Third NC; Fourth NC	
	2071-2100	+3.3	+6.2	Third NC; Fourth NC	
RCP8.5 / CCSM4	up to 2040	+1.7	-5.7	Third NC; Fourth NC	Armenia
	2041-2070	+3.2	+16.3	Third NC; Fourth NC	
	2071-2100	+4.7	+2.9	Third NC; Fourth NC	
RCP8.5 / METRAS	up to 2040	+1.4	-2.7	Fourth NC	Armenia
	2041-2070	+3.1	-5.4	Fourth NC	
	2071-2100	+4.5	-8.3	Fourth NC	

As we can see from the figures in the table above, the temperature projections obtained using different scenarios and models are close to each other. On the other hand, precipitation projections vary greatly.

1.4 Algorithms and Models used for Water Resources Vulnerability Assessments in Armenia

For the study, assessment and forecasting of water resources vulnerability to climate change, the IPCC (Intergovernmental Panel on Climate Change) has provided some guidelines. They recommend using physical-statistical or process genetic theoretical models that allow assessing the vulnerability of water resources to climate change through the existing relationships between individual elements of water resources and the climatic factors conditioning them.

The process genetic models are based on established physical laws and theories, expressing the dynamics of interactions between climate and its impact object. The impact of climate and other factors on the formation of water resources is different in different river basins in mountainous countries; therefore, theoretical or process-based models are not currently applicable in practice.

The physical - statistical models are based on statistical interconnections between climate and its impact object. Besides, they establish correlations between individual elements of water resources and the main factors that underlie them. There is a wide range of uses of physical - statistical models, from one-dimensional regression model to multidimensional models, with the help of which a number of estimates and forecasts are made.

The assessment of the change and vulnerability of the RA water resources due to climate change have been carried out using physical-statistical or regression models in all papers, which provide sufficient accuracy of vulnerability assessment in the mountainous conditions of our country. It allows establishing correlations between the river flow and climate elements, such as precipitation and air temperature. The physical-statistical or regression model has the following standard form:

$$W = K_1X + K_2T + B$$

where:

W- is the river flow, m^3/sec ,
X- is total precipitation, mm ,
T- is air temperature, $^{\circ}C$,
B- is a constant of the equation,
*K*₁ and *K*₂ - are coefficients.

Along with the physical-statistical or regression models, the DSS (decision support system) models created in the GIS (Geographic Information System) have also been used and reported in the literature.

Due to the complexity of separating atmospheric precipitation (snow, rain and sleety shower) and implementing snow-measuring works in the river basins, as well as the availability of air temperature data in the territory of the Republic, depending on the forecasted climate changes, the possible changes in the river flow characteristics of Armenia were evaluated in the following order:

- Data missing in the series of multi-year observations at hydrological observation stations and meteorological stations in river basins were restored: the series observed for up to 20 years is considered short and it is inappropriate to establish correlations between hydrometeorological elements. Therefore, the series were extended to 40-50 years. The data of missing months in the year series were also restored.
- With the help of graphical relationships between the absolute elevations of hydrological observation stations and meteorological stations and their data the average weighted values for precipitation, evapotranspiration and river flow in the river basins were determined;
- Graphical relationships were established between the data of the hydrological observation stations and the meteorological stations of the river basins.

Methodology of Assessment of Lakes' and Reservoirs' Vulnerability

For assessment of the changes and vulnerability of water resources in lakes and reservoirs due to climate change in the Republic, observed air temperature, precipitation, river flow and evapotranspiration data were used.

To determine the value of evaporation from the surface of the water mirror of lakes and reservoirs the empirical formulas used for mountainous areas, the evapotranspiration maps compiled in the past for the Republic were used, or new graphical relationships were compiled between the total evapotranspiration and absolute elevations of meteorological stations located nearby lakes and reservoirs.

The average annual flows of the rivers that flow into and out of the reservoir or lake were determined, taking into account the values of abstractions and water releases, according to water use permits. The average annual atmospheric precipitation on the surface of the reservoir or lake mirror was determined, according to the data of meteorological stations located nearby the water body.

Methodology of calculation of river basin water balance

The purpose of water balance calculation is the quantitative assessment, accounting, management and planning of the water resources of river basin in its natural state.

The water balance of the river basins of Armenia was prepared based on the method proposed by M.I. Lvovich. The river basin water balance was determined by the following equation, expressed quantitatively between precipitation, evaporation and flow:

$$X = E + Y_{nf}.$$

where:

X – is precipitation, mm,

E – is total evapotranspiration, mm,

Y_{nf} – is the natural flow (which is equal to $Y_{nf} = Y_{rf} \pm Y_{df}, Y_{rf}$), mm, and *Y_{df}* – is the deep flow, mm.

Determination of precipitation - Graphical relationships were established between the precipitation values measured in the meteorological stations of the river basin and the absolute elevation of the stations. From the average weighted elevation of the river basin from the graphical relationship, the average value of precipitation (X) was determined.

Determination of total evapotranspiration – The values of total evapotranspiration (E) were mainly calculated by the following equation by A. Valesyan:

$$E = E_g[(1+0.07 (V_i - V_{ave}))H_{ave}/ H_i]$$

where:

E – is the average monthly total evapotranspiration, mm,

E_g – is monthly evapotranspiration (determined by graphical relationship between precipitation and air temperature), mm,

V_i – is the average monthly wind velocity at the meteorological station, m/sec,

V_{ave} – is the average monthly wind velocity in the Republic, established at 3.3 m/sec,

H_{ave} – is the average value of atmospheric pressure in the Republic, established at 605 mm,

H_i – is the average value of atmospheric pressure for the given month in the meteorological station.

The total evapotranspiration of river basin was estimated by compiling graphical relationship between the total evapotranspiration values estimated in the meteorological stations and the values of their absolute elevations. From the average weighted elevation of the river basin from the graphical relationship, the average value of precipitation (X) was determined.

Determination of natural river flow – The difference between the precipitation and total evapotranspiration from water balance is used to determine the total (climatic) flow - $Y_{nf} = X - E$.

The natural flow is divided into natural and deep river flows: $Y_{nf} = Y_{rf} + Y_{df}$.

In order to determine the natural river flow (Y_{rf}), first, the actual river flow at the river basin hydrological observation stations is brought to natural.

The actual river flow is brought to natural by using the equation of channel and water balances.

The formula has the following standard form:

$$Y_{rf} = Y_i + Y_a - Y_b - V_c + E \pm \Delta S_{res},$$

where:

Y_i – is the actual flow in the hydrological observation station,

Y_a – is the water abstraction,

Y_b – is the return water from water abstraction,

V_c – is the transfer of water from one river basin to another,

ΔS_{res} – is the change (use or storage) of water reserve in reservoirs,

E – is the amount of evaporation from the water surface of the reservoir.

The data on the amount of abstraction and the return water from abstraction are taken from the Water Use Permits issued by the WRMA of the RA Ministry of Environment. In case the water use permits do not include the amount of return water from the abstraction, it is calculated based on the results of the investigations carried out at the Water Problems and Hydraulic Engineering Institute. According to these results, the average volume of return water from irrigation in the territory of the Republic is about 20% of the abstracted water and 70% of water abstracted for industry and household purposes.

Thereafter, a graphical relationship is drawn between the values of the river flow brought to natural in hydrological observation stations and the absolute elevations of the hydrological observation stations. Placing the weighted elevation of the river basin from the graphical relationship on the graph, we determine the average natural river flow of the river basin.

Determination of deep flow – The deep flow is determined by the difference of the natural flow and the natural river flow: $Y_{df} = Y_{nf} - Y_{rf}$.

Water balance estimation for mountainous regions is usually associated with a number of difficulties resulting not only from climatic and hydrological data for high mountainous regions, but also from harsh climatic conditions in mountainous regions. These regions have complex geological and hydrogeological structure, which makes the flow redistribution accounting into surface and deep flows difficult. The surface watershed line of the river basin usually does not correspond to the deep flow formation area.

In the early studies, for assessment of the vulnerability of water resources from the climate change linear regression equations were mostly used that included the air temperature, precipitation, and river flow.

Started from the 2009, in several studies GIS-based models were used for vulnerability assessment which allows incorporating more factors (especially, Digital Elevation Model (DEM) and its derivatives) in calculations. GIS-based Decision Support System developed within USAID Clean Energy and Water Project has a Climate Change module that can analyze historical trends in climatic parameters and project the surface natural flow for the selected river basin using user-defined emission scenarios and projection periods. The system uses not only linear, but also power, logarithmic, and exponential equations. The output of the projection is the raster model of surface natural flow where for each raster cell has a projected value of surface flow. This model is used for the vulnerability assessment in frames of the projects on Southern, Sevan, and Hrazdan River Basin Management Plan development.

For the vulnerability assessment in Arpa River Basin, **Water Evaluation and Planning Tool (WEAP)** developed by the Stockholm Environment Institute was tested within the study “Vulnerability of Water Sector due to the Climate Change” (2012) conducted in the scope of “Enabling Activities for the Preparation of Armenia’s Third National Communication to the UNFCCC’s Third National Communication to the UNFCCC” UNDP/GEF/00060737 Project. The results are presented in the Third National Communication. WEAP operates on the basic principle of a water balance and can be applied to municipal and agricultural systems, a single watershed or complex transboundary river basin systems.

The main difficulty in using the complex hydrologic models like WEAP is their high requirements to input parameters. We can expect a representative output from that models only in the case if we have the accurate and reliable data on hydro-meteorological parameters, hydrogeology (infiltration coefficient, porosity, deep flow, etc.), soil composition, vegetation, as well as water use. Therefore, it is necessary to conduct studies aimed to the identification of available data sources for hydrological modeling. Based on the results of those studies, the priorities in hydro-meteorological and hydrogeological monitoring network upgrade, hydrogeological, soil, vegetation and other research for the data obtaining for hydrological modeling will be identified.

In scope of the study on “Climate Change Analysis for Ararat Valley” (USAID ASPIRED Project, 2018), vulnerability assessment of water resources of the Ararat Valley’s watershed has been implemented using the **Climate Change Model of Decision Support System (DSS)** ArcGIS extension calibrated within the frames of the USAID ASPIRED Project. The input data for the assessment are hydro-meteorological observations data, GIS layers of meteorological stations, hydroposts locations and sub-catchment areas within the studied territory.

In the Climate Change Model of DSS, firstly, annual temperature, precipitation, snowfall and surface natural flow data for the period of 1961-2016 loaded into the attribute tables of Meteo Stations and Hydroposts GIS layers (Figure 3).

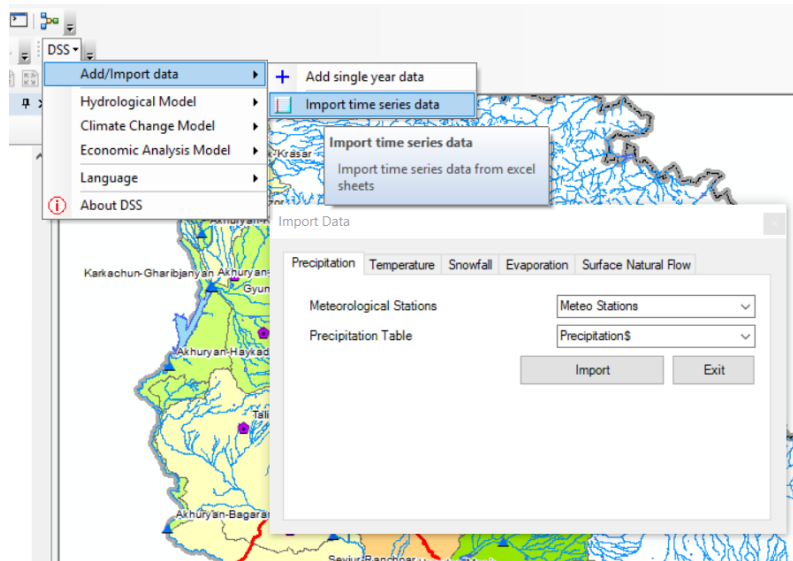


Figure 3. Import of Hydro-Meteorological Time Series Data from Excel Sheets to the GIS Layers

Climate Change model consists of two component – Historic Trends and Projections (Figure 4).

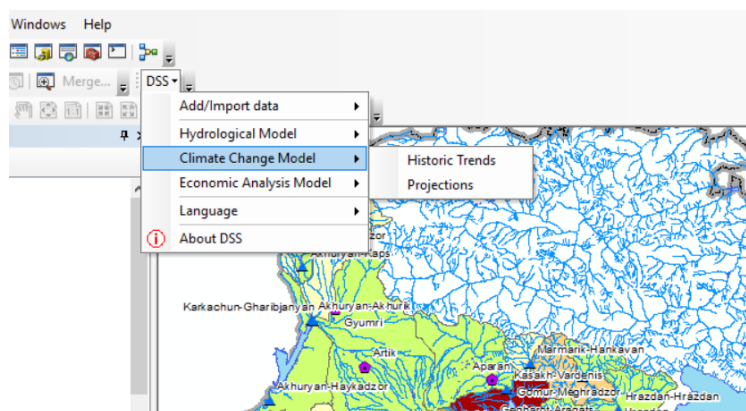


Figure 4. Decision Support System (DSS) Extension of ArcGIS

In Historic Trends component, changes in annual precipitation, snowfall and surface natural flow compared between WMO-established baseline period (1961-1990) and analysis period (in this case - 1991-2016).

Baseline period, the 30-year period of consecutive records of historic climate data, is considered long enough to smooth out year to year variations, including wet, dry, warm and cool periods. According to the WMO and IPCC, this period represents the climate before significant changes attributable to human activity were detected.

Thus, the model calculates the annual average value of a given parameter for the period of 1961-1990, and assesses the deviation of values for the period of 1991-2016 against the baseline period average values.

Historic trends component window and example of graphs are presented below (Figure 5).

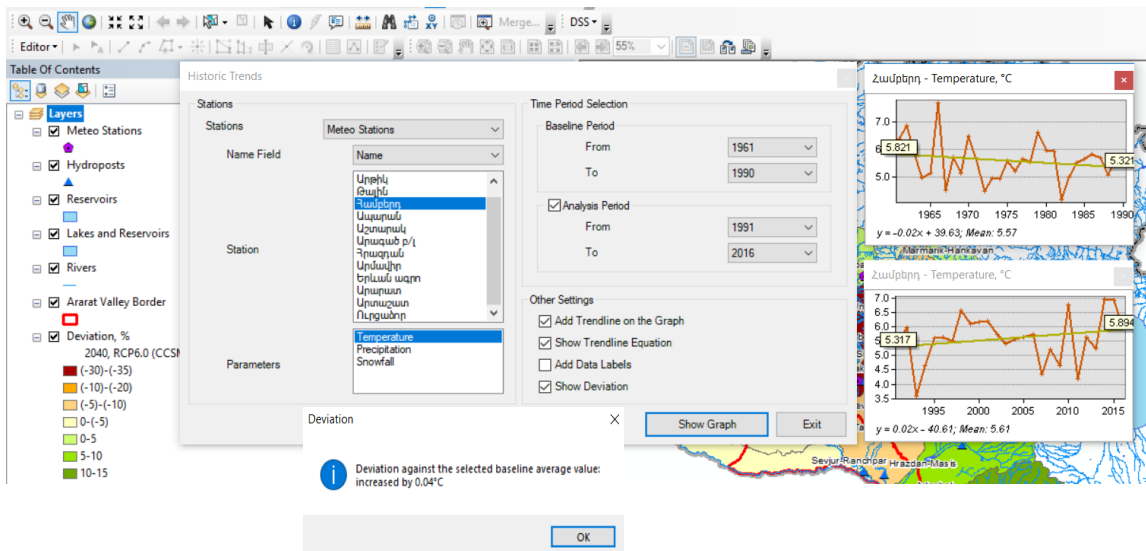


Figure 5. Historic Trends Component of DSS

The Projections component of the Climate Change Model aims at modelling of future picture of natural flow under the IPCC scenarios in order to give an understanding on further water availability and design respective plan of measures and adaptation.

The input data of Projections component are the layers of meteo stations and hydroposts loaded with hydro-meteorological observation data for the period of 1961-2016 and layer of the catchment areas sub-catchments within the studied territory.

Baseline period, against which the deviation of surface natural flow is calculating; Basin/River Basin; Emission Scenario and Time Horizon of projection should be selected for the calculation of projected surface natural flow (Figure 6).

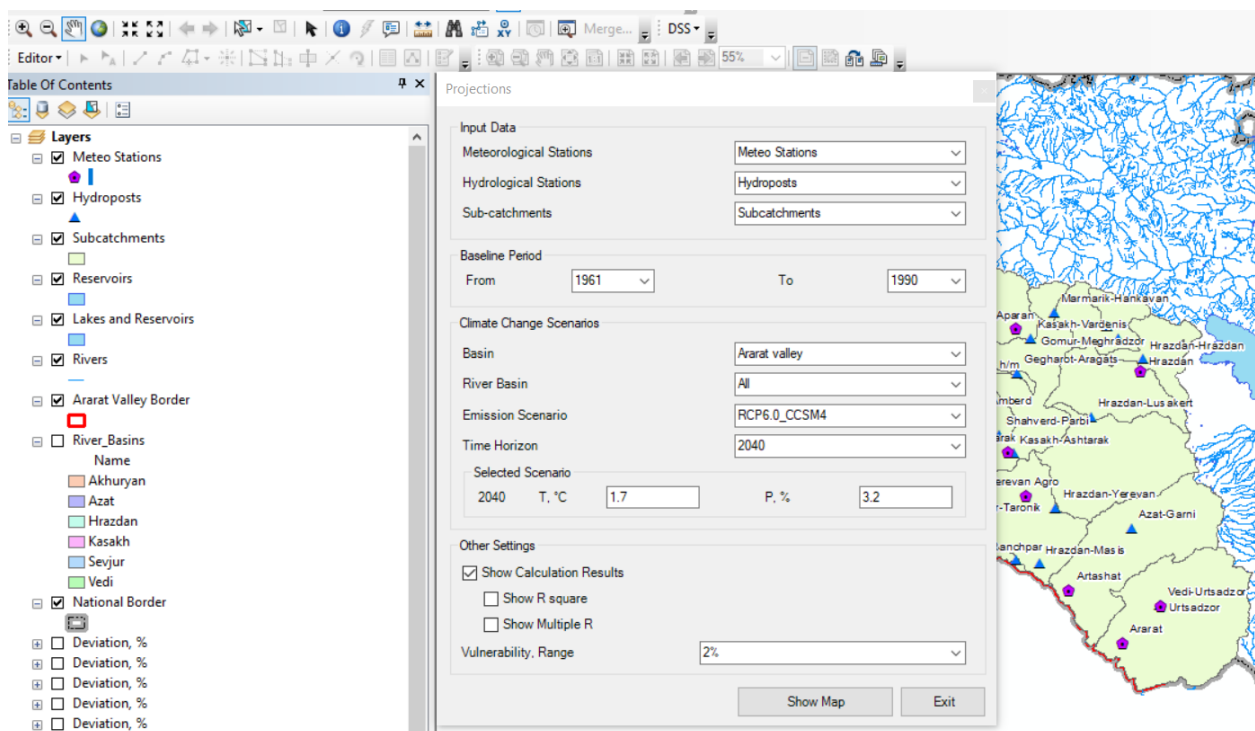


Figure 6. Projections Component of DSS

The output of the calculation is the layer of sub-catchments classified by the ranges of projected changes in surface natural flow for selected scenario and period. Columns with deviation percent and projected values of surface natural flow are also added to the Hydroposts layer (Figure 7).

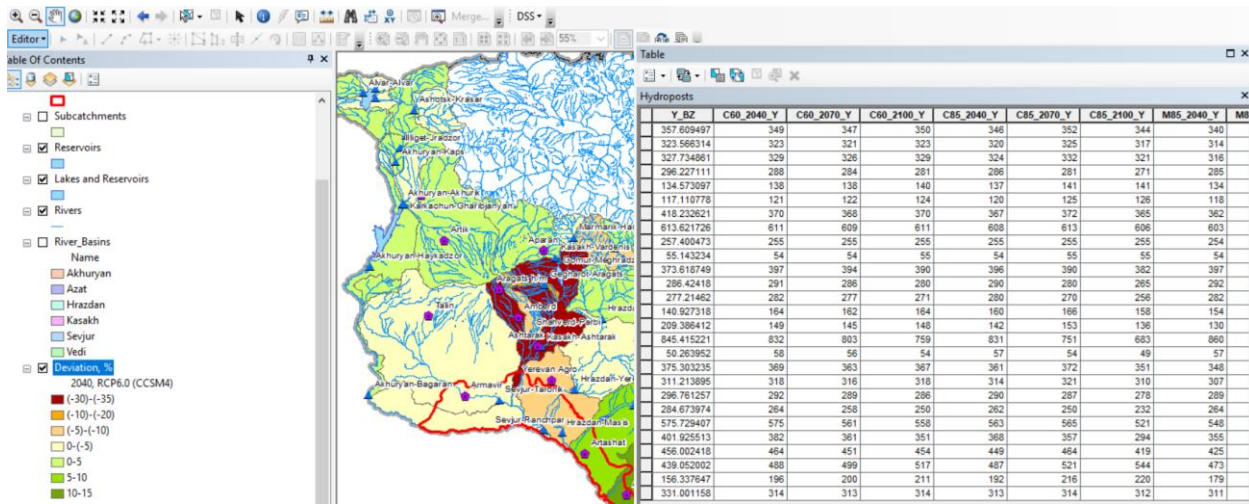


Figure 7. Example of the Output of Projections Component of DSS

DSS Climate Change Model has been also used for Sevan and Hrazdan basin vulnerability assessments within the development of draft management plans for those basins (EUWI+, 2020).

Analysis of the vulnerability assessments presented in the report “Stocktaking exercise to identify legal, institutional, vulnerability assessment and adaptation gaps and barriers in water resources management under climate change conditions” showed that there are issues related to the baseline river flow data that does not allow to adequately compare the results of those assessments. The main issue is that not in all assessments the restored natural flow for baseline period (1961-1990) was used. Quality of natural flow restoration is another issue. There are methodological shortcomings in the calculations for bringing the river flow to the natural flow at the hydrological observation stations.

- There are no actual water use data in the country. In the former USSR, water use data, such as the abstraction and disposal, were mandatorily recorded in water use logs, based on which the actual river flow restored to the natural flow had near-to-natural accuracy. As for the actual flow brought to the natural at present, it has deviations, resulting in an inaccurately estimated natural flow that cannot be used to have an accurate picture for assessment and forecast of climate change.
- While bringing the river flow to natural flow for the rivers, on which relatively large reservoirs were built, the amount of evaporation from the surface of the reservoir mirror was not taken into account.

1.5 Development of Water Resources Vulnerability Map for Armenia

As mentioned above, in the latest studies the temperature and precipitation projections have been obtained using IPCC RCP6.0 and RCP8.6 scenarios and CCSM4 and METRAS models. These studies include:

- “The Vulnerability Assessment of Water Resources of the Republic of Armenia under the Climate Change”, UNDP-GEF, 2018;
- “Climate Change Analysis for Ararat Valley”, USAID ASPIRED Project, 2019;

- “Draft Basin Management Plan for Lake Sevan Basin in Armenia”, EUWI+ Project, 2020;
- “Draft Basin Management Plan for Hrazdan River Basin in Armenia”, EUWI+ Project, 2020.

In the “The Vulnerability Assessment of Water Resources of the Republic of Armenia under the Climate Change” (2018), the vulnerability assessment has been conducted for 25 hydroposts, Lake Sevan, and 4 reservoirs (Akhuryan, Marmarik, Aparan, and Azat) (Table 2).

Table 2. Projected Changes of the Flow of Main Rivers in Armenia (IPCC RCP8.5 Scenario, METRAS Model)

Hydropost Name	Scenario	River flow, million m ³	Flow change		Period
			million m ³	%	
Pambak-Tumanyan	Baseline	335.4	0	0	
	T+1.4, 0.97Q	308.7	-26.8	-7.98	2011-2040
	T+3.1, 0.95Q	273.5	-61.9	-18.5	2041-2070
	T+4.5, 0.92Q	241.6	-93.9	-28.0	2071-2100
Debed-Ayrum	Baseline	1053.0	0	0	
	T+1.4, 0.97Q	928.5	-124.5	-11.8	2011-2040
	T+3.1, 0.95Q	794.8	-258.2	-24.5	2041-2070
	T+4.5, 0.92Q	675.5	-377.5	-35.9	2071-2100
Dzoraget-Gargar	Baseline	479.9	0	0	
	T+1.4, 0.97Q	407.0	-43.3	-9.6	2011-2040
	T+3.1, 0.95Q	317.0	-133.3	-29.6	2041-2070
	T+4.5, 0.92Q	239.5	-210.8	-46.8	2071-2100
Aghstev-Ijevan	Baseline	296.4	0	0	
	T+1.4, 0.97Q	289.3	-7.06	-2.38	2011-2040
	T+3.1, 0.95Q	281.3	-15.1	-5.08	2041-2070
	T+4.5, 0.92Q	271.6	-24.7	-8.35	2071-2100
Hakhum-Tsaghkavan	Baseline	49.4	0	0	
	T+1.4, 0.97Q	35.0	-14.4	-29.1	2011-2040
	T+3.1, 0.95Q	19.5	-29.9	-60.6	2041-2070
	T+4.5, 0.92Q	6.32	-43.1	-87.2	2071-2100
Getik-Gosh	Baseline	109.5	0	0	
	T+1.4, 0.97Q	95.7	-13.8	-12.6	2011-2040
	T+3.1, 0.95Q	74.9	-34.6	-31.6	2041-2070
	T+4.5, 0.92Q	56.6	-52.8	-48.3	2071-2100
Tavush-Berd	Baseline	18.4	0	0	
	T+1.4, 0.97Q	17.8	-0.62	-3.38	2011-2040
	T+3.1, 0.95Q	17.2	-1.21	-6.58	2041-2070
	T+4.5, 0.92Q	16.7	-1.69	-9.15	2071-2100
Araks-Surmalu	Baseline	2660.3	0	0	
	T+1.4, 0.97Q	2324.6	-335.7	-12.6	2011-2040
	T+3.1, 0.95Q	1965.4	-694.9	-26.1	2041-2070
	T+4.5, 0.92Q	1654.8	-1005.5	-37.8	2071-2100
Akhuryan-Akhurik	Baseline	225.7	0	0	
	T+1.4, 0.97Q	213.5	-13.8	-6.08	2011-2040
	T+3.1, 0.95Q	200.3	-27.0	-11.9	2041-2070
	T+4.5, 0.92Q	187.7	-39.6	-17.4	2071-2100
Kasakh-Ashtarak	Baseline	112.8	0	0	
	T+1.4, 0.97Q	89.9	-22.9	-20.3	2011-2040
	T+3.1, 0.95Q	61.8	-51.0	-45.2	2041-2070
	T+4.5, 0.92Q	38.2	-74.5	-66.1	2071-2100

Hrazdan-Hrazdan	Baseline	242.4	0	0	
	T+1.4, 0.97Q	186.0	-56.4	-23.3	2011-2040
	T+3.1, 0.95Q	117.0	-125.4	-51.7	2041-2070
	T+4.5, 0.92Q	58.3	-184.2	-76.0	2071-2100
Marmarik-Hankavan	Baseline	54.4	0	0	
	T+1.4, 0.97Q	49.4	-5.04	-9.27	2011-2040
	T+3.1, 0.95Q	43.7	-10.7	-19.7	2041-2070
	T+4.5, 0.92Q	38.6	-15.8	-29.0	2071-2100
Dzknaget-Tsovagyugh	Baseline	34.2	0	0	
	T+1.4, 0.97Q	29.1	-5.08	-14.8	2011-2040
	T+3.1, 0.95Q	22.3	-11.9	-34.8	2041-2070
	T+4.5, 0.92Q	16.3	-17.9	-52.3	2071-2100
Masrik-Tsovak	Baseline	97.9	0	0	
	T+1.4, 0.97Q	93.8	-4.09	-4.18	2011-2040
	T+3.1, 0.95Q	90.8	-7.06	-7.21	2041-2070
	T+4.5, 0.92Q	88.6	-9.25	-9.45	2071-2100
Vardenis-Vardenik	Baseline	56.1	0	0	
	T+1.4, 0.97Q	35.9	-20.1	-35.9	2011-2040
	T+3.1, 0.95Q	24.9	-31.2	-55.6	2041-2070
	T+4.5, 0.92Q	14.0	-42.1	-75.0	2071-2100
Martuni-Geghhovit	Baseline	55.7	0	0	
	T+1.4, 0.97Q	49.9	-5.80	-10.4	2011-2040
	T+3.1, 0.95Q	45.7	-10.0	-18.0	2041-2070
	T+4.5, 0.92Q	41.9	-13.8	-24.8	2071-2100
Argichi-Verin Getashen	Baseline	193.2	0	0	
	T+1.4, 0.97Q	151.7	-41.5	-21.5	2011-2040
	T+3.1, 0.95Q	108.9	-84.3	-43.7	2041-2070
	T+4.5, 0.92Q	72.6	-120.6	-62.4	2071-2100
Bakhtak-Tsakkar	Baseline	21.8	0	0	
	T+1.4, 0.97Q	17.7	-4.13	-18.9	2011-2040
	T+3.1, 0.95Q	12.8	-9.06	-41.5	2041-2070
	T+4.5, 0.92Q	8.52	-13.3	-60.9	2071-2100
Gavaraget-Noratus	Baseline	105.3	0	0	
	T+1.4, 0.97Q	105.7	0.40	0.38	2011-2040
	T+3.1, 0.95Q	103.1	-2.21	-2.10	2041-2070
	T+4.5, 0.92Q	100.9	-4.45	-4.22	2071-2100
Azat-Garni	Baseline	138.3	0	0	
	T+1.4, 0.97Q	135.8	-2.51	-1.81	2011-2040
	T+3.1, 0.95Q	132.1	-6.22	-4.49	2041-2070
	T+4.5, 0.92Q	128.6	-9.70	-7.02	2071-2100
Vedi-Urtsadzor	T+1.4, 0.97Q				
	T+3.1, 0.95Q	53.6	-4.26	-7.36	2011-2040
	T+4.5, 0.92Q	49.6	-8.26	-14.3	2041-2070
	T+1.4, 0.97Q	46.2	-11.7	-20.2	2071-2100
Arpa-Jermuk	Baseline	167.7	0	0	
	T+1.4, 0.97Q	152.0	-15.7	-9.34	2011-2040
	T+3.1, 0.95Q	133.7	-33.9	-20.2	2041-2070
	T+4.5, 0.92Q	117.8	-49.8	-29.7	2071-2100
Meghriget-Meghri	Baseline	93.8	0	0	
	T+1.4, 0.97Q	89.6	-4.20	-4.47	2011-2040
	T+3.1, 0.95Q	81.0	-12.8	-13.6	2041-2070

Voghji-Kapan	T+4.5, 0.92Q	73.1	-20.8	-22.1	2071-2100
	Baseline	379.6	0	0	
	T+1.4, 0.97Q	244.7	-134.9	-35.5	2011-2040
	T+3.1, 0.95Q	135.8	-243.8	-64.2	2041-2070
Vorotan-Gorhayk	T+4.5, 0.92Q	97.1	-282.5	-74.4	2071-2100
	Baseline	116.6	0	0	
	T+1.4, 0.97Q	108.4	-8.23	-7.06	2011-2040
	T+3.1, 0.95Q	97.5	-19.1	-16.4	2041-2070
	T+4.5, 0.92Q	87.9	-28.7	-24.6	2071-2100

In the “Climate Change Analysis for Ararat Valley” (2019), the vulnerability of water resources of the Ararat Valley’s watershed area has been assessed. Natural river flow changes have been projected for 27 hydroposts located within the Akhuryan, Sevjur, Kasakh, Hrazdan, Azat, and Vedi river basins (Table 3).

Table 3. Projected Changes of the Surface Natural Flow in the Watershed Area of Ararat Valley under the IPCC RCP8.5 Scenario (IPCC RCP8.5 Scenario, METRAS Model)

Hydropost Name	Baseline Average SNF, mm	2011-2040		2041-2070		2071-2100	
		Projected SNF, mm	Deviation, %	Projected SNF, mm	Deviation, %	Projected SNF, mm	Deviation, %
Sevjur-Taronik	405	397	-1.9	388	-4.1	380	-5.9
Sevjur-Ejmiatsin	305	292	-4.1	277	-9.1	264	-13.3
Sevjur-Ranchpar	295	282	-4.2	267	-9.3	255	-13.6
Kasakh-Vardenis	163	154	-5.5	149	-8.7	143	-12
Kasakh-Ashtarak	219	205	-6.2	189	-13.5	175	-19.9
Gegharot-Aragats	926	860	-7.1	778	-15.9	713	-23
Shahverd-Parbi	63	57	-7.9	51	-17.3	46	-25.3
Hrazdan-Hrazdan	362	348	-3.8	333	-7.9	318	-11.9
Hrazdan-Lusakert	314	307	-2.3	299	-4.6	292	-7
Hrazdan-Yerevan	297	289	-2.4	281	-5.2	274	-7.7
Hrazdan-Masis	280	264	-5.6	246	-12.2	230	-17.8
Marmarik-Hankavan	582	548	-5.7	511	-12	477	-17.9
Marmarik-Aghavnadzor	405	355	-12.2	298	-26.2	248	-38.7
Gomur-Meghradzor	457	425	-6.9	390	-14.5	357	-21.7
Azat-Garni	450	473	5.2	503	11.8	526	17
Vedi-Urtsadzor	172	179	4.4	189	10.6	197	14.7
Alvar-Alvar	314	311	-0.8	309	-1.4	307	-1.9
Akhuryan-Paghakn	353	340	-3.7	335	-5.2	329	-6.7
Akhuryan-Amasia	323	314	-2.9	308	-4.5	303	-6.2

Akhuryan-Kaps	326	316	-3	309	-5.2	301	-7.4
Akhuryan-Akhurik	294	285	-2.9	276	-6.2	267	-9.2
Akhuryan-Haykadzor	134	134	0.5	136	1.4	136	1.9
Akhuryan-Bagaran	117	118	1.6	121	3.7	122	5.3
Dzoraget-Dzorakert	379	362	-4.3	358	-5.4	354	-6.5
Ashotsk-Krasar	622	603	-3	598	-3.7	594	-4.4
Illiget-Jradzor	254	254	0.3	254	0.2	254	0
Karkachun-Gharibjanyan	54	54	0	54	0.1	54	0

In the “Draft Basin Management Plan for Hrazdan River Basin in Armenia” (2020), Hrazdan basin’s vulnerability has been assessed for 11 hydroposts within the basins of the rivers flowing into Lake Sevan (Table 4).

Table 4. Projected Changes in Annual Surface Natural Flow, % (IPCC RCP8.5 Scenario, METRAS Model)

River-Post	RCP8.5		
	2040	2070	2100
Kasakh-Vardenis	-11,6	-25,4	-37,1
Kasakh-Ashtarak	-10,1	-22,2	-32,3
Gegharot-Aragats	-7	-15,8	-22,8
Hakhverd-Parpi	-7,4	-16,2	-23,7
Hrazdan-Hrazdan	-4,1	-8,7	-12,8
Hrazdan-Lusakert	-4,3	-9,3	-13,7
Hrazdan-Yerevan	-3,4	-7,3	-10,7
Hrazdan-Masis	-6,1	-13,3	-19,4
Marmarik-Hankhavan	-5,5	-11,8	-17,4
Marmarik-Aghavnadzor	-3	-6,2	-9,3
Gomur-Meghradzor	-1,3	-2,5	-3,9

In the “Draft Basin Management Plan for Sevan River Basin in Armenia” (2020), Hrazdan basin’s vulnerability has been assessed for 12 hydroposts within Hrazdan and Kasakh river basins (Table 5).

Table 5. Projected Changes in Annual Surface Natural Flow, % (IPCC RCP8.5 Scenario, METRAS Model)

River-Post	RCP8.5		
	2040	2070	2100
Pambak-Pambak	0.8	1.7	2.5
Dzknaget-Tsovagyugh	-19.7	-42.7	-62.8
Drakhtik-Drakhtik	-20.3	-44.4	-64.8
Masrik-Tsovak	3.4	7.9	11.1
Karchaghbyur-Karchaghbyur	-12.3	-27.3	-39.6
Vardenis-Vardenik	3.5	8.3	11.7
Martuni-Geghhovit	0.2	1	1.1

Argichi-Verin Getashen	-17.5	-38.4	-56
Tsaghkashen-Vaghashen	-13.3	-28.9	-42.5
Lichk-Lichk	10.3	22.9	33.1
Bakhtak-Tsakkar	-2.2	-4.9	-7.2
Gavaraget-Noratus	0.7	1.5	2.3

In the current study, we compared, analyzed, and summarizes the results of the studies that used METRAS model to create a comprehensive basin-level vulnerability map for Armenia.

The results are presented in the Table 6 and Figure 8.

Table 6. Vulnerability of Water Resources in Armenia due to the Climate Change (IPCC RCP8.5 Scenario, METRAS Model)

BMA	Basin/Watershed Area	2040	2070	2100
Akhuryan	r. Sevjur	-4.2	-9.3	-13.6
Akhuryan	r. Araks	-12.6	-26.1	-37.8
Akhuryan	Lower flow of Akhuryan River	1.6	3.7	5
Akhuryan	Middle flow of Akhuryan River	-2.9	-6.2	-9.2
Akhuryan	Upper flow of Akhuryan River	-2.9	-4.5	-6.2
Akhuryan	r. Mantash (Karkachun)	0	0.1	0
Araratyan	r. Azat	-1.81	-4.49	-7.02
Araratyan	r. Vedi	-7.36	-14.3	-20.2
Araratyan	r. Arpa	-9.34	-20.2	-29.7
Hrazdan	Lower flow of Hrazdan River	-5.6	-12.2	-17.8
Hrazdan	Middle flow of Hrazdan River	-2.4	-5.2	-7.7
Hrazdan	Upper flow of Hrazdan River	-3.8	-7.9	-11.9
Hrazdan	Upper flow of Kasakh River	-5.5	-8.7	-12
Hrazdan	Middle and lower flows of Kasakh River	-6.2	-13.5	-19.9
Hrazdan	r. Marmarik	-9.3	-19.7	-29
Northern	r. Pambak	-7.98	-18.5	-28
Northern	r. Aghstev	-2.38	-5.08	-8.35
Northern	r. Tavush, Hakhindja	-3.38	-6.58	-9.15
Northern	r. Dzoraget	-9.6	-29.6	-46.8
Northern	r. Debed	-11.8	-24.5	-35.9
Northern	r. Getik	-12.6	-31.6	-48.3
Northern	r. Hakhum	-29.1	-60.6	-87.2
Sevan	Lake Sevan	-12.3	-23.8	-33.8
Sevan	r. Dzknaget, north-western shore of Lake Sevan	-19.7	-42.7	-62.8
Sevan	r. Gavaraget	0.38	-2.1	-4.2
Sevan	r. Masrik	-4.18	-7.21	-9.45
Sevan	Eastern shore of Lake Sevan	-13.1	-28.5	-41.7
Sevan	Western and south-western shore of Lake Sevan	-10.5	-23.2	-34.1
Sevan	Southern shore of Lake Sevan	-10.6	-16.1	-21.7
Sevan	r. Karchaghbyur	-12.3	-27.3	-39.6
Sevan	r. Argichi	-19.5	-41.1	-59
Southern	r. Vorotan	-7.06	-16.4	-24.6
Southern	r. Voghji	-35.5	-64.2	-74.4
Southern	r. Meghriget	-4.47	-13.6	-22.1

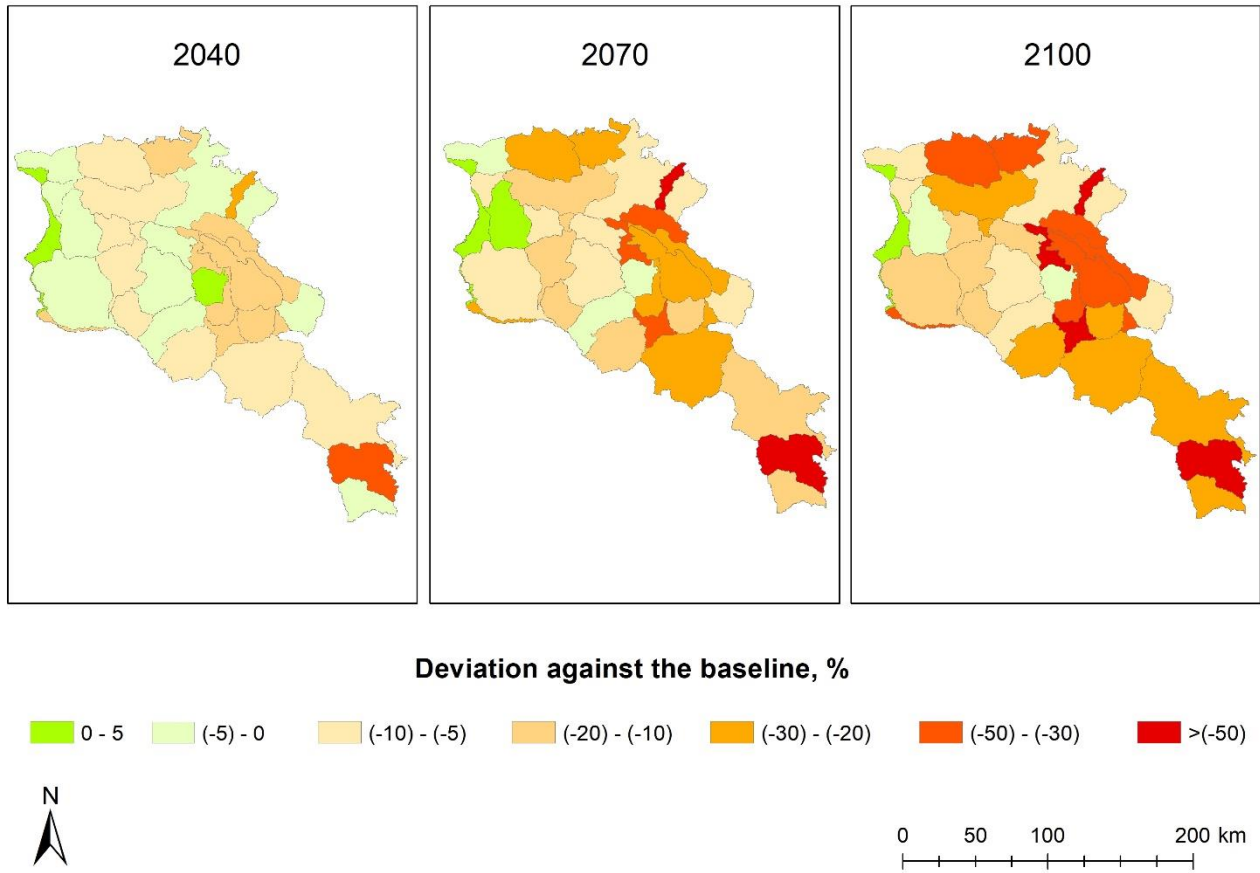


Figure 8. Water Resources Vulnerability due to Climate Change, IPCC RCP8.5 Scenario, METRAS Model

2. Specific recommendations on tools, algorithms and remote sensing data to be applied for water resources vulnerability assessment in Armenia and preparation of vulnerability map of water resources due to climate change

2.1 Remote Sensing in Climate Change Studies

Remote sensing techniques, and specifically satellite images, have been effectively used in a wide range of climate change studies connected with water resources vulnerability assessment, such as for:

- investigating global temperature trends, both at the ocean surface and in the atmosphere,
- detecting changes in solar radiation affecting global warming,
- monitoring aerosols, water vapour concentration, and changes in precipitation regime,
- studying the dynamics of snow extension and ice cover,
- monitoring sea-level changes and coastal modifications,
- monitoring vegetation status and change,
- monitoring water resources and impact due to droughts and dry periods,
- monitoring fire events and fire emissions,
- predicting disaster risk, such as floods and drought,
- guiding decision-making processes on climate change adaptation.

The use of remote sensed data is quickly evolving, both in terms of available techniques and resolution, and other uses relevant for climate change adaptation are expected to emerge in the next future.

Some concerns, however, have been posed on the use of remote sensing. Studying and monitoring climate change require long-term time series of observations, while satellite data are often available for short-term period. Furthermore, some uncertainties and distortions of received image frames due to vibrations and turbulence can derive by biases in sensors and retrieval algorithms, so the use of satellite observations in climate change studies requires a clear identification of such limitations. Other possible limitations include:

- (i) high cost for acquiring aircraft and drone high-resolution data;
- (ii) in some cases, limited access to needed technologies due to costs or skills constrains;
- (iii) temporal discontinuity of aircraft and satellite data; while the first can be particularly expensive and therefore available for a limited number of surveys, the second are collected at fixed intervals depending on the satellite return time.¹

2.2 Basics of Water Resources Vulnerability Assessment: Hydrologic Cycle and Water Balance Models

The IPCC (2018) defines vulnerability as “the degree to which a system is able or unable to cope with the adverse effects of climate change, including climate variability and extreme effects”. Vulnerability

¹ [Climate ADAPT: Use of remote sensing in climate change adaptation \(2019\)](#)

is a function of the character, magnitude and rate of climate change to which a system is exposed, its sensitivity and its adaptive capacity. In the area of water resource vulnerabilities, researchers define the term in relation to the physical, biological, socio-economic and ecological conditions of the environment, the policy decisions and the regulatory framework for water protection (Allier et al., 2008; Sinan et al., 2003; Wang et al., 2012).

In all water resource vulnerability research, the vulnerability of water resources is defined in relation to internal and/or external factors. The conceptualization in water resources vulnerability assessment is based on the choice of factors considered relevant (Idé et al., 2019).

Several authors conceptualize vulnerability in different ways, but this difference lies in the fact that the factors that influence the risk of vulnerability of water resources are numerous and require a relevant choice by scientists in conceptualizing vulnerability. IPCC (2018) points out that many specialists in different fields have conceptualized vulnerability according to their areas of intervention, based on the objectives to be achieved and the methodologies applied.

In the water resources vulnerability assessment, the choice of factors is one of the most important steps. There are a number of methods for selecting the right factors (Organization for Economic Cooperation and Development, OECD, 2008; Hinkel et al., 2011, Adger, 2006, and other) and their relative weights [Statistical methods: principal component analysis; Participatory methods (GIZ, 2014; OECD, 2008); “Budget Allocation Process (BAP)”]; Public opinion]. This is an opinion poll addressed to the public, focusing on the notion of concern. Methods such as expert opinion or Delphi technique, deductive approach, LR, empiric approach and analytic hierarchy process (AHP) are also used to weight factors (Idé et al., 2019).

Algorithms, models, and tools for the assessment of the water resources vulnerability to the climate change are mainly based on the water balance estimation. Water balance represents the water cycle within the environment (Figure 9). Water balance can be estimated for the catchment, river or lake basin, sea basin, etc.

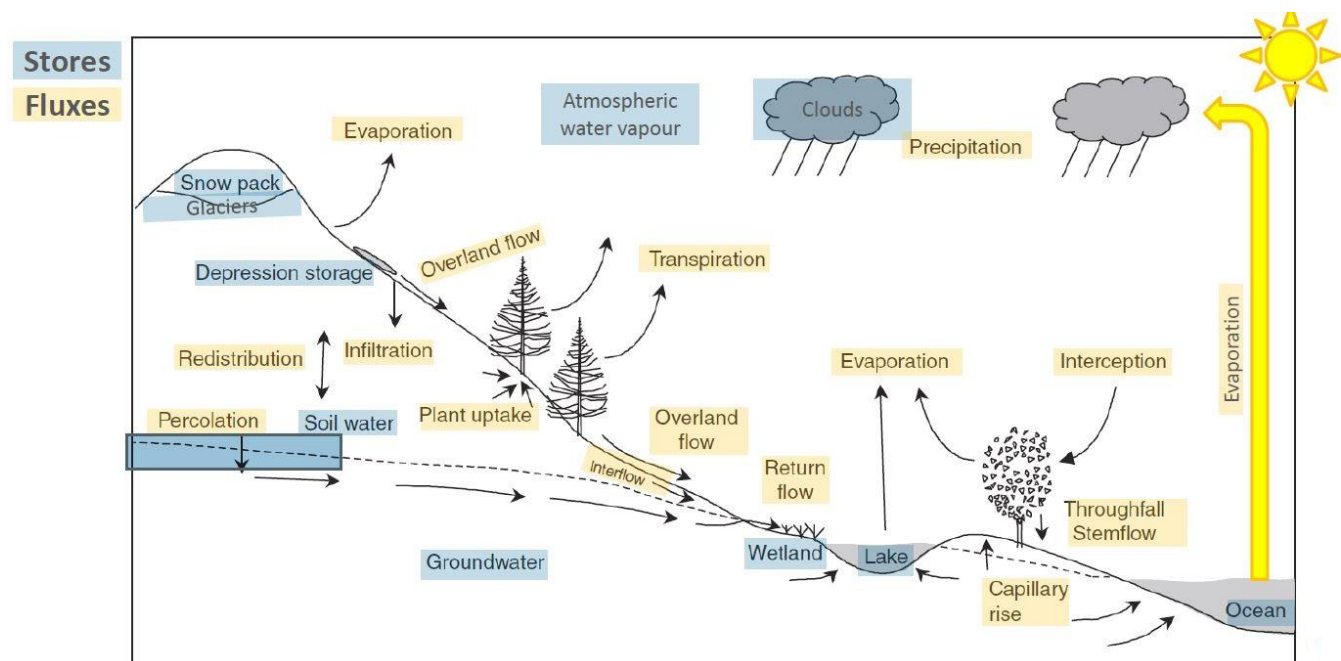


Figure 9. The Global Water Cycle. Source: Technical University of Wien

Annual flux rates within global water (hydrological) cycle is strongly connected to the energy cycle and carbon cycle.

The energy cycle includes:

- evapotranspiration
- ocean-atmospheric circulations
- Global warming (atmospheric H₂O)

The carbon cycle includes:

- Photosynthesis/ vegetation growth
- Carbon sequestration (dissolving in oceans)
- Heterotrophic respiration

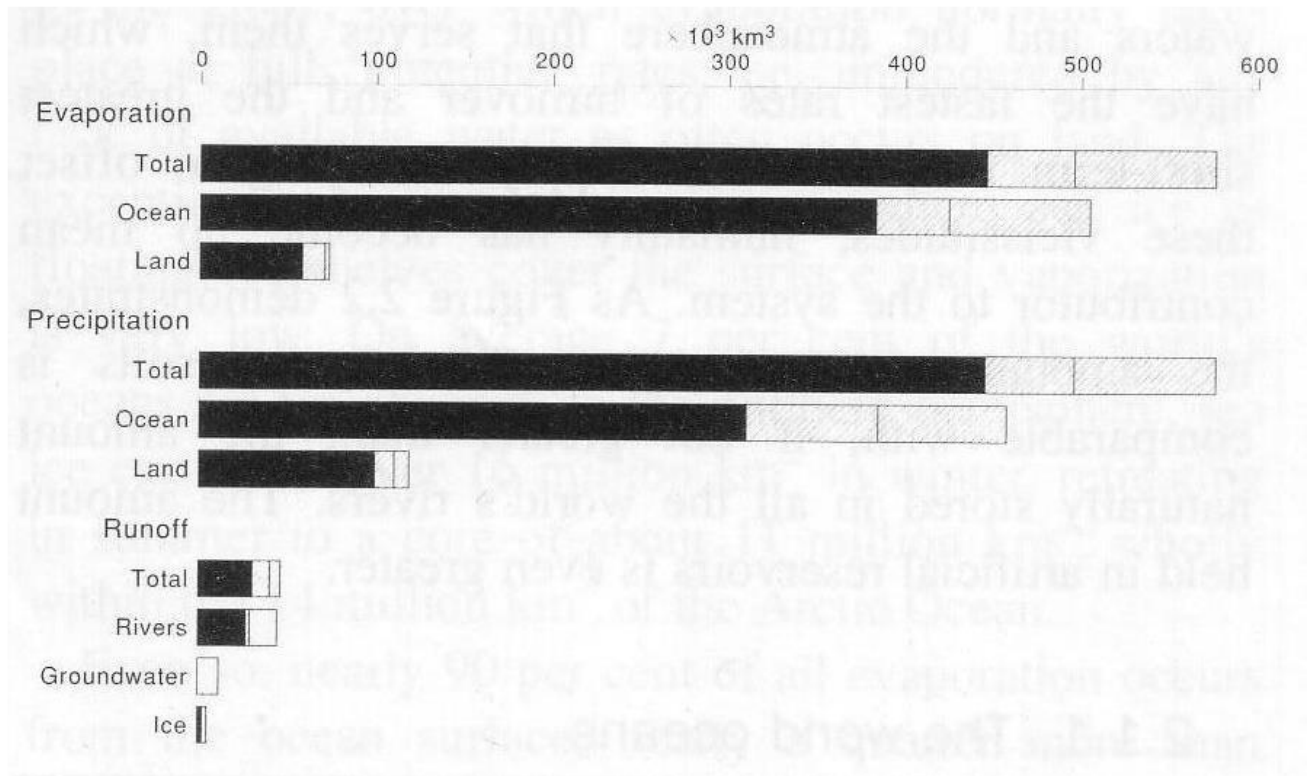


Figure 10. Elements of the Global Water Cycle. Source: Jones, 1997

Remote Sensing techniques (satellite data) is being used for the observations of different components of the water cycle:

- Oceans & inland surface waters (rivers, lakes, seas, etc.): extent, ocean color, quality (turbidity), temperature, wind, water depth, water level, salinity, etc.
- Atmosphere: clouds, precipitation, water vapor, etc.
- Snow: snow area, snow water equivalent, freeze/thaw, etc.
- Ice sheets and glaciers: elevation, area, flow (speed/direction), freeze/thaw, snow cover, etc.
- Land: soil moisture, groundwater, evapotranspiration, wetlands, irrigation, etc.

Based on the availability, quality, and adequacy of the data, the water balance can be assessed by the algorithms, models, and tools of different complexity.

The simplest water balance model can be presented as:

$$\Delta S = P - ET - R,$$

where ΔS is a change in storage, P is a precipitation, E is an evapotranspiration, and R is an runoff.

A little bit more complicated is the following equation:

$$\Delta GW + \Delta SM = P+I - ET - R,$$

where GW is a groundwater, SM is a soil moisture, and I is an irrigation.

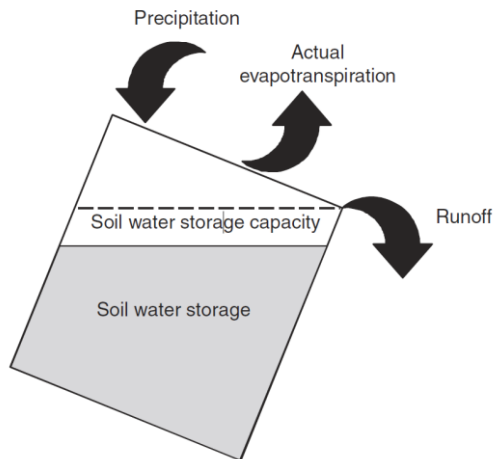


Figure 11. A Simple Representation of Water Balance Model. Source: Technical University of Wien

There are also more sophisticated models that require more datasets and, potentially, have a capability to produce more accurate results and projections.

Based on the review of international practice, the most frequently used methods for water resources vulnerability assessment due climate change are:

- Parametric methods or overlay and index methods;
- Process-based models or methods by physical modeling;
- Statistical methods.

SWAT (Soil and Water Assessment Tool), WEAP (Water Evaluation and Planning) and similar small watershed to river basin-scale hydrological models are being widely used in different countries to evaluate the observed and projected climate change impacts on the quantitative and qualitative characteristics of water resources. Retrospective analysis using the hydro-meteorological observational data usually conducted for testing and calibration of those models for the local conditions of studied basins and returns reliable results in case of sufficient and accurate actual input data. Thus, most uncertain and sensitive factors in the assessment of the vulnerability of water resources to climate change are the projected values of the temperature and precipitation according to the various scenarios of IPCC. This means that the greatest effort should be made to improve GCMs and methods for statistical downscaling of GCM simulations.

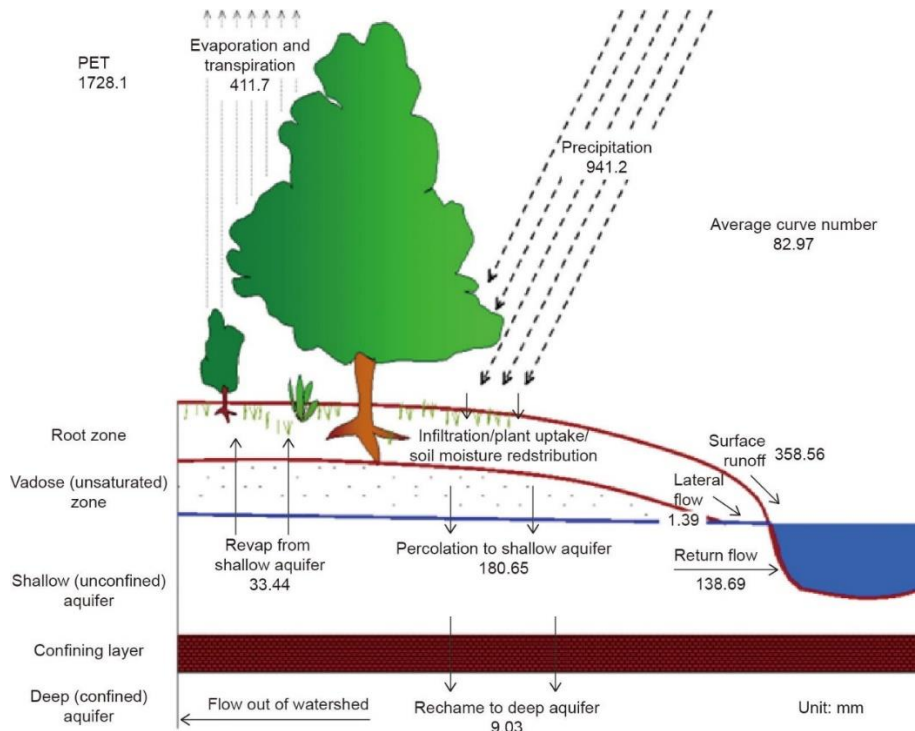


Figure 12. SWAT Model Inputs and Output (Shivhare et al., 2018)

A comprehensive review on assessing the vulnerability of water resources in the context of climate change in small watersheds using SWAT is presented in Marin et al. (2020).

List of selected publications on WEAP application for water resources vulnerability assessment is presented here: <http://www.weap21.org/index.asp?action=216>.

There are also some studies where combination of SWAT and WEAP models for water supply-demand analysis, for example, “Water Supply and Demand Under Climate Change Impacts and Management Options in Tributary Basin of Tonle Sap Lake, Cambodia” (Touch et al., 2020) (Figure 13).

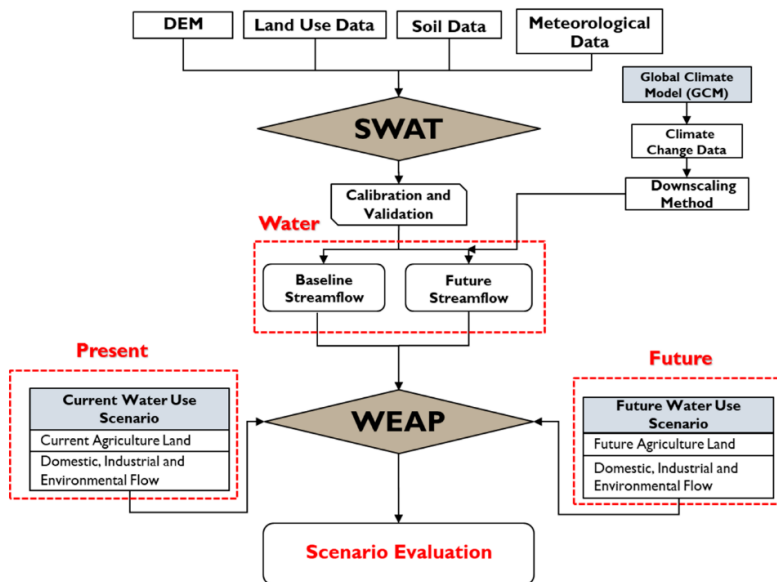


Figure 13. Model flowchart that illustrates the integration of the Soil and Water Assessment Tool (SWAT) and Water Evaluation and Planning (WEAP) models

Precipitation, evapotranspiration, land surface temperature, soil moisture, leaf area index, land use / land cover and other parameters can be obtained through satellite products and fill the input data gaps in these models enhancing the accuracy of results. The better results could be achieved when we calibrate the satellite data using the ground-based monitoring data (hydro-meteorological observations, field studies of land cover, etc.). However, some parameters, such as hydrogeology and soil composition, are not possible or very hard to obtain from satellite imagery.

Most of the sensors are already in place for meteorology, hydrology, and climatology, as documented by the Observing Systems Capability Analysis and Review (OSCAR, <https://www.wmo-sat.info/oscar/>) tool of the World Meteorological Organization (WMO), which defines the requirements for the observation of physical variables. The Global Climate Observing System (GCOS, <https://gcos.wmo.int/en/home>) maintains the definitions and observation needs (GCOS, 2016) of the Essential Climate Variables (ECVs)² required to systematically observe the Earth's changing climate. Ground-based observations produce datasets for estimates of changes in the hydrological cycle and for deriving trends (Groisman et al., 2004), but this happens only in limited areas of the world, where the observing networks are dense enough and ensure adequate quality standards (Levizanni et al., 2019).

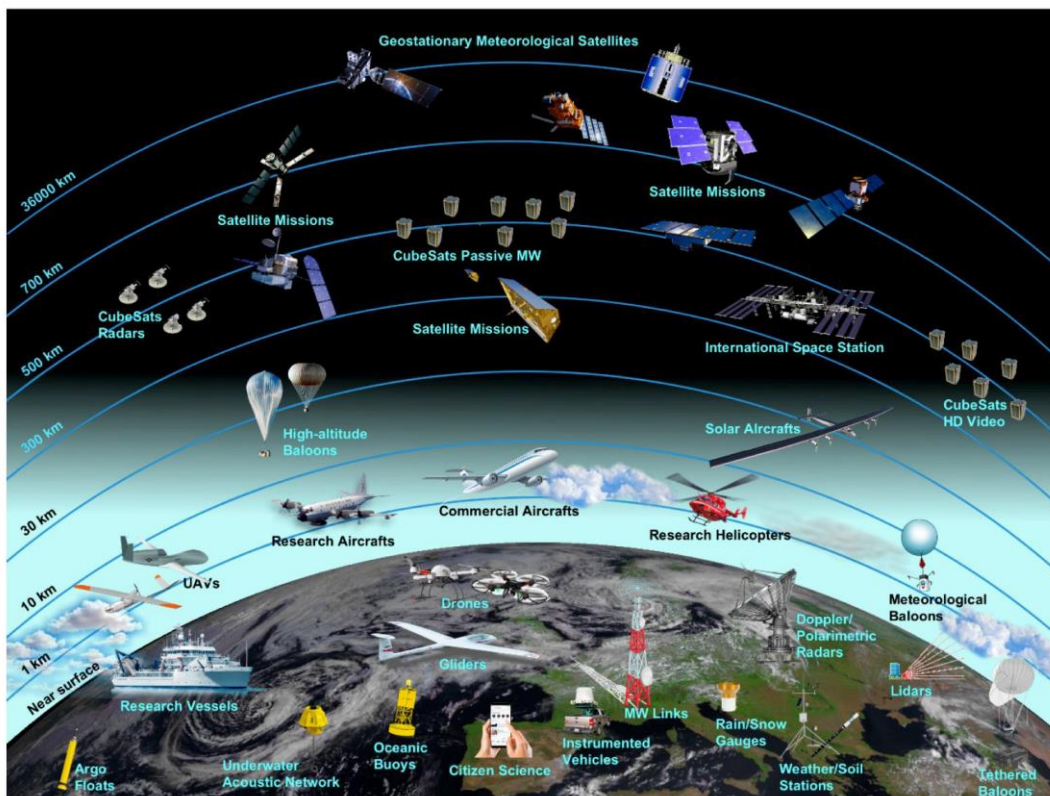


Figure 14. The Global Observing System of the Water Cycle

Hydrological cycle is potentially constrained by the carbon cycle and vice versa, and multiple observation sources can be used to constrain land surface models in order to mitigate bias from any single data type (Haverd et al., 2013).

It is essential to obtain robust and physically sound figures of the response of the water cycle to climate change. Accurate modeling is fundamental to disentangling the effects of radiative forcing by

² <https://public.wmo.int/en/programmes/global-climate-observing-system/essential-climate-variables>

greenhouse gases on the water cycle components on the regional and global levels (Harding et al., 2011).

In particular, attention is to be paid to local changes in precipitation and its extremes that depend upon small changes in large-scale atmospheric circulation, as well as regional feedback mechanisms. Allan et al. (2014) argue that climate modeling may have insufficient predictive capabilities to determine such responses at the scale required by impact models. This calls for the determination of robust, large-scale responses in the hydrological cycle across models (Held et al., 2006), which is still not satisfactory, especially regarding the representation of clouds and microphysical processes, rainfall variability, and the influence of land–atmosphere coupling on rainfall patterns and their variability (Martin et al., 2014; Sorooshian et al., 2008; Tang et al., 2016).

An increase in model spatial resolution, encouraged by enhanced computer power, would seem to be a reasonable way forward, but a recent study (Benedict et al., 2019) showed that a straightforward resolution increase in global hydrological models is most likely not the best solution to improve discharge predictions, thus emphasizing the role of a better representation of processes and of improved parameterizations.

An acceleration of the water cycle is generally predicted by all models, but not enough is known of the physical mechanisms behind the phenomenon (Feng et al., 2014). Precipitation does not tell the whole story of hydrological changes; in particular, it may obscure the fact that in a warmer world, more precipitation will lead to regions getting more rain, but others not getting enough to keep pace with the growing evaporative demand (Sherwood, 2014). The use of drought indices has recently produced contradictory results concerning model outputs predicting that dry regions will become drier and wet regions wetter (the DDWW paradigm), showing that DDWW theory is more useful when only precipitation is considered, while proving less conclusive when also evapotranspiration and soil conditions are integrated (Yang et al., 2019).

Soil moisture memory seems to be large enough so that Diermeyer et al. (2009) suggest that the real-time monitoring and accurate model initialization of land surfaces in forecast models could help improving medium-range weather and sub-seasonal climate forecasts. At the same time, surface ocean salinity observations have shown that the water cycle has amplified at less than the Clausius-Clapeyron (CC) rate following recent global warming, thus adding confidence to projections of the total water cycle change under greenhouse gases emission scenarios (Skirris et al., 2016).

In this perspective, high-resolution estimates of the terrestrial water and energy storages are necessary to overcome the lack of reliable land–surface fields available globally and in near-real time.

This requires the integration of data from advanced observing systems (Wulfmeyer et al., 2018) and modeling community efforts, as in the case of the Global Land Data Assimilation System (GLDAS) (Rodell et al., 2004), in order to make sense of the large amount of observation data which is available nowadays (Lahoz et al., 2010; Margulis et al., 2006).

All authors point out several key limitations in the quantitative appraisal due to unrealistic model results and incomplete and unsatisfactory global observational datasets. However, the combination of ground-based and remote sensing data is considered a way to reduce sampling issues, both in space and, progressively, in time (Schneider et al., 2017). Significant uncertainties are associated with state-of-the-art climate datasets when examining so-called “macroweather” (from a few months to a few decades) precipitation variability (Nogueira, 2019).

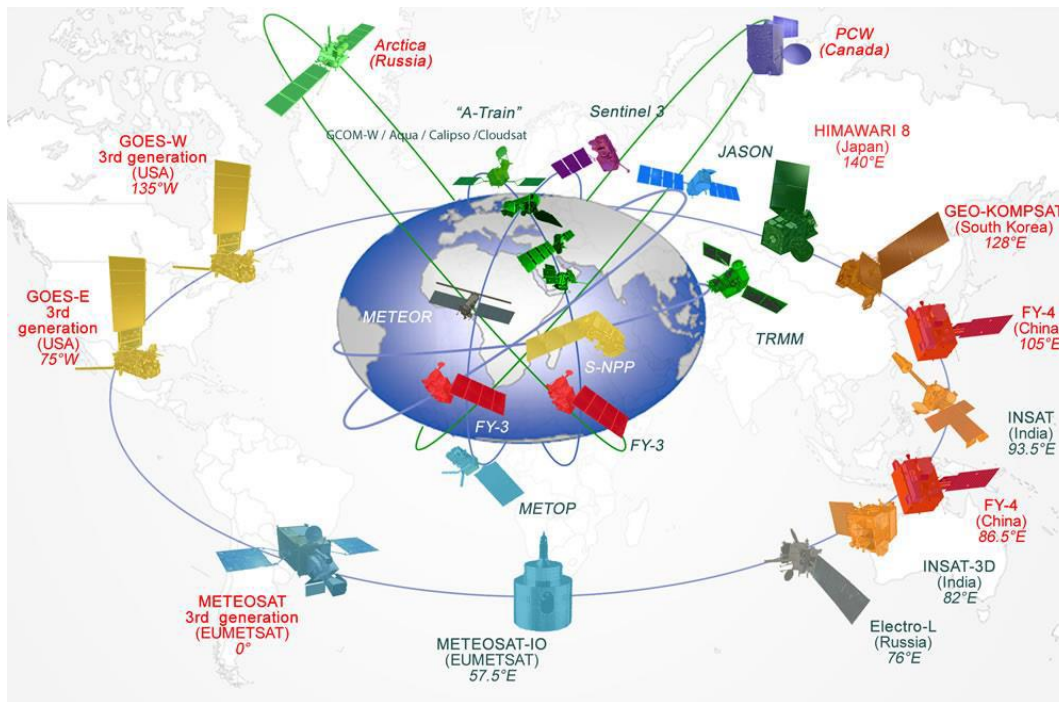


Figure 15. Meteorological Satellite Network

2.3 Satellite Measurement of Precipitation

A general improvement of the observational capabilities for the constant monitoring of precipitation will substantially contribute to the investigation of climate change processes. Measuring precipitation from space has been a key application of passive remote sensing since the early days of satellite meteorology in the 1960s.

The evolution of satellite observational capabilities in recent times is shown in Figure 16.

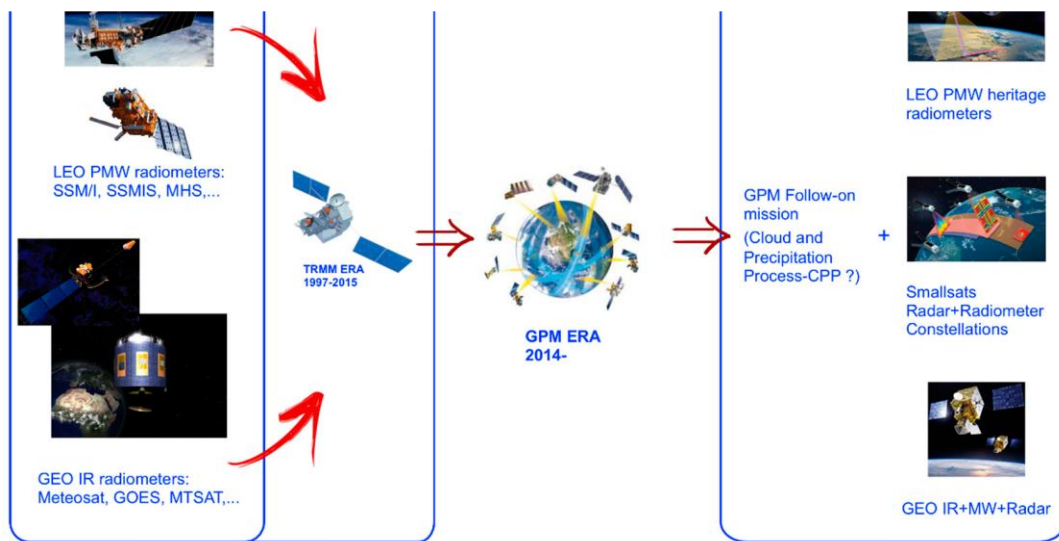


Figure 16. Evolution of the satellite constellation for precipitation measurements

There are several initiatives aimed at the development of the reliable, long term, consistent global precipitation datasets that can be used for more accurate projecting of future precipitation and improving the GCMs and RCMs. Three datasets of this type are described below.

2.3.1 TAMSAT

TAMSAT* enhances the capacity of African meteorological agencies and other organizations by providing and supporting the use of satellite-based rainfall estimates and related data products.

TAMSAT produces daily rainfall estimates for all of Africa at 4km resolution. The TAMSAT archive spans 1983 to the delayed present. The longevity of the dataset makes it especially suitable for risk assessment. Applications of the data include famine early warning, drought insurance and agricultural decision support.

Rainfall estimates and other TAMSAT products are issued on the 1st, 6th, 11th, 16th, 21st, and 26th of the month. All TAMSAT data are released for operational, research and commercial use under a creative commons license.

TAMSAT was established by the University of Reading in 1977. In the last three years, the group has developed close collaborations with the Climate Division of the National Centre for Atmospheric Science ([NCAS](#)) and the National Centre for Earth Observation ([NCEO](#)) to extend the range of climate services it provides. These collaborations are supporting the development of new datasets and other products, including rainfall estimate uncertainties, full column soil moisture, and probabilistic forecasts of drought.

TAMSAT product uses the Cold Cloud Duration approach that estimates precipitation through calibration with ground data.

*TAMSAT stands for Tropical Applications of Meteorology using SATellite data and ground-based observations (<https://www.tamsat.org.uk/>).

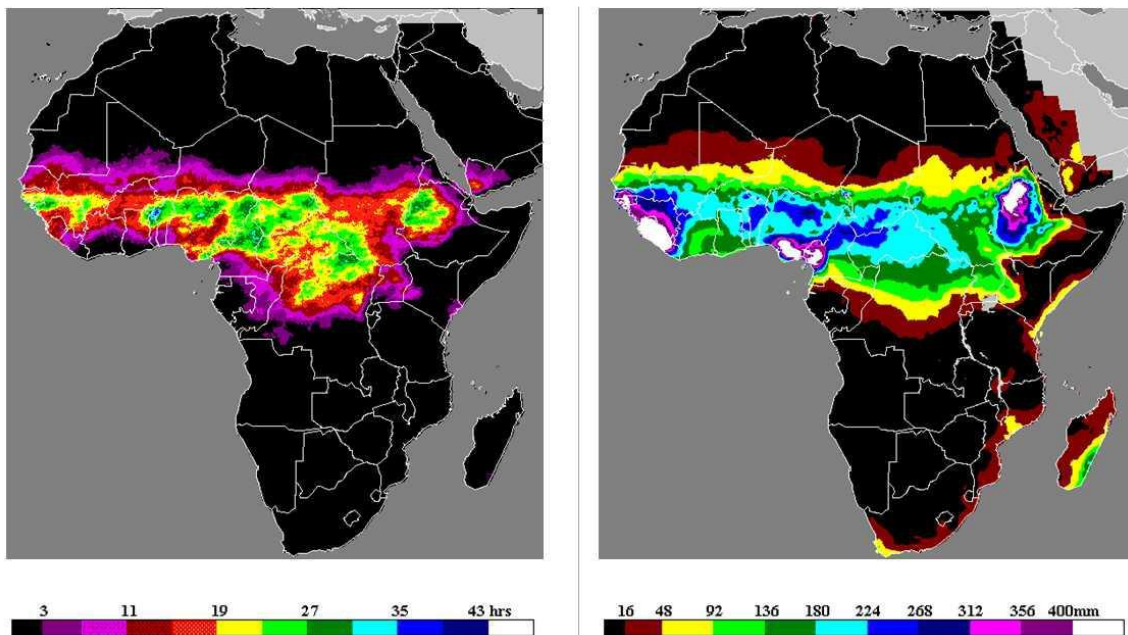


Figure 17. Comparison of monthly Cold Cloud Duration map of Africa (left) with long term mean of precipitation interpolated from raingauges (right).

2.3.2 NOAA Operational GCOM-W1 AMSR-2 Products System

The GCOM-W project is a 13-year mission with a series of three satellites that aims to measure global-scale water-cycle changes over a long period of time. The GCOM-W1 is the first satellite in the GCOM-W series and was launched in May 2012 by the Japan Aerospace Exploration Agency (JAXA). AMSR2 onboard the GCOM-W1 satellite will continue Aqua/AMSR-E observations of water vapor, cloud liquid water, precipitation, sea surface temperature, sea surface wind speed, sea ice concentration, snow depth, and soil moisture.

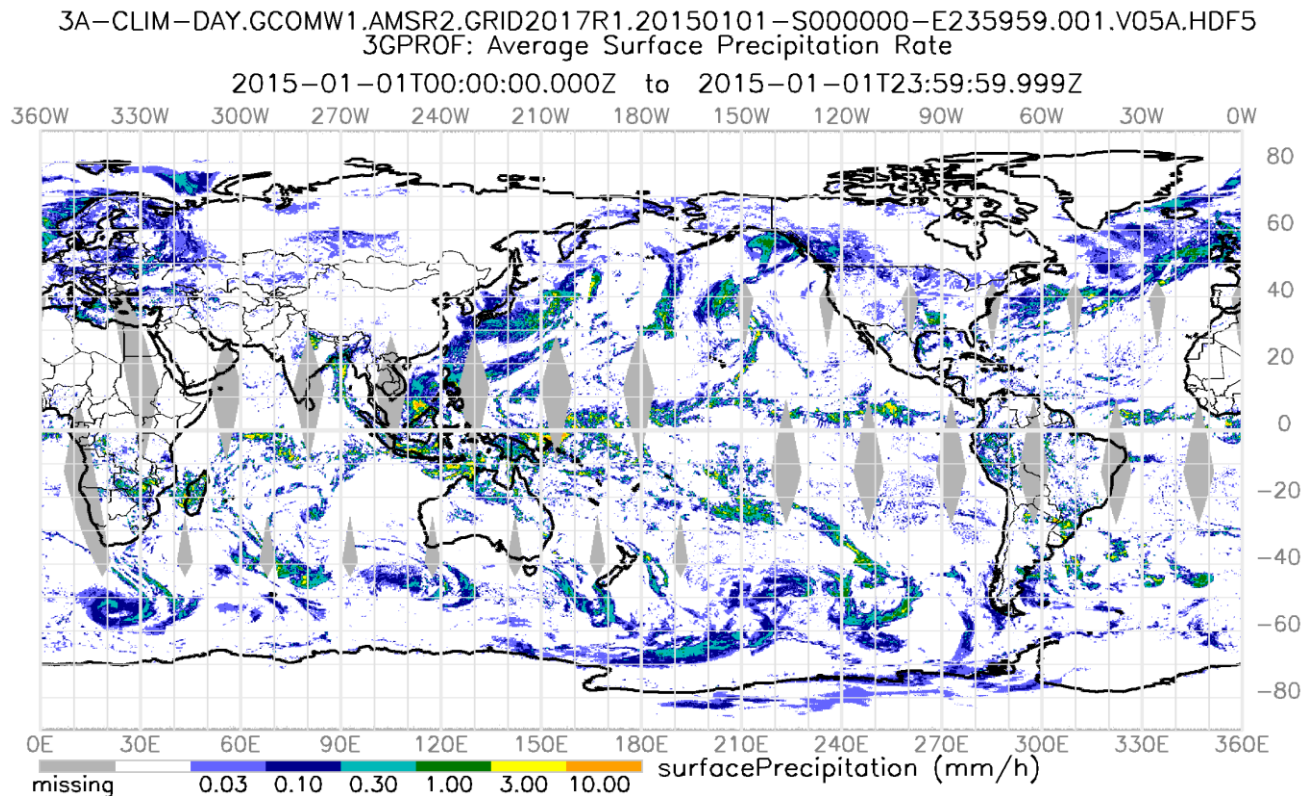


Figure 18. Global rain rate in mm/h derived from AMSR2, a passive microwave radiometer on board of JAXA's GCOM W1 satellite (<https://disc.gsfc.nasa.gov>)

2.3.3 Tropical Rainfall Measuring Mission (TRMM)

TRMM was a research satellite in operation from 1997 to 2015, designed to improve our understanding of the distribution and variability of precipitation within the tropics as part of the water cycle in the current climate system. By covering the tropical and sub-tropical regions of the Earth, TRMM provided much needed information on rainfall and its associated heat release that helps to power the global atmospheric circulation that shapes both weather and climate. In coordination with other satellites in NASA's Earth Observing System, TRMM provided important precipitation information using several space-borne instruments to increase our understanding of the interactions between water vapor, clouds, and precipitation, that are central to regulating Earth's climate.

TRMM was a mission with a circular orbit at an altitude of 350 km and an inclination of 35°. It has carried multiple instruments:

- TRMM Microwave Imager (TMI)
- Precipitation Radar (PR)
- Visible and Infrared Scanner (VIRS)
- Clouds and the Earth's Radiant Energy System (CERES)
- Lightning Imaging Sensor (LIS)

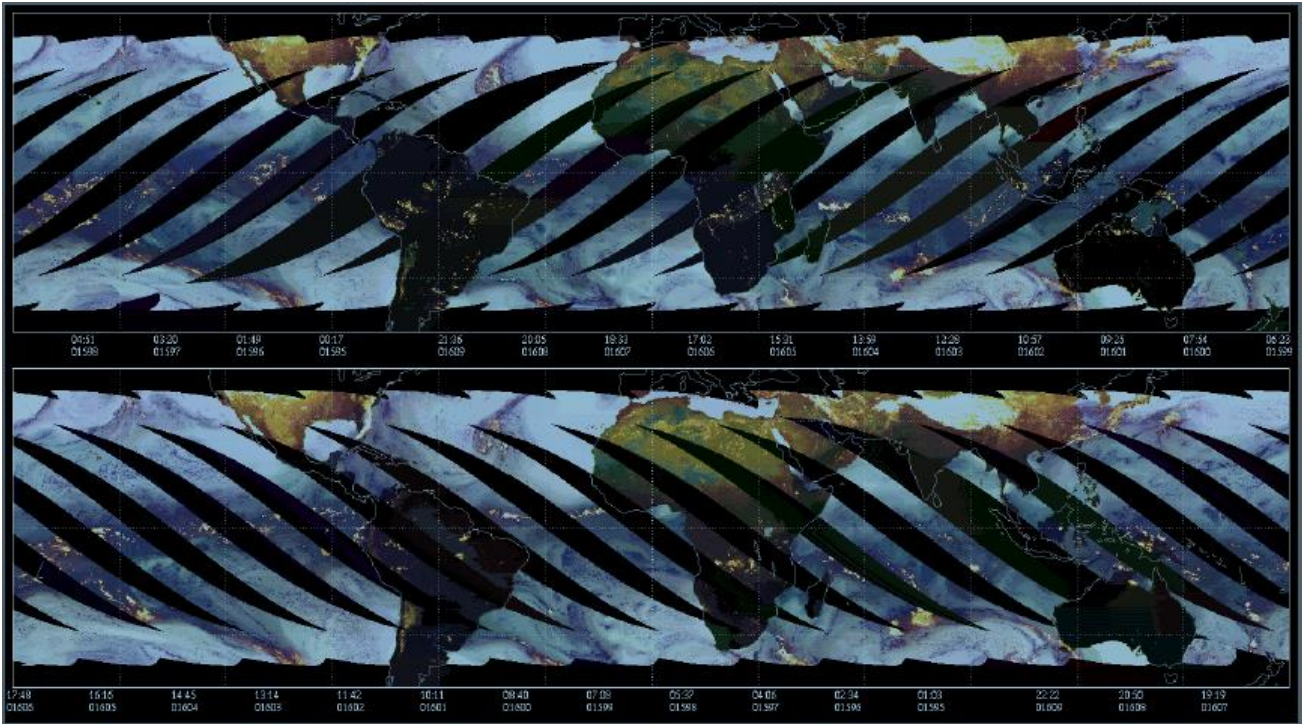


Figure 19. TMI: Passive microwave sensor that measures in five frequencies: 10.7 (45 km spatial resolution), 19.4, 21.3, 37, and 85.5 GHz (5 km spatial resolution). Swath width 780 km.

The 10.7 GHz frequency provides a linear response to rainfall (<https://gpm.nasa.gov/missions/trmm>).

2.4.4 TRMM Multi-satellite Precipitation Analysis (TMPA)

The Tropical Rainfall Measuring Mission (TRMM) Multi-satellite Precipitation Analysis (TMPA) is intended to provide a “best” estimate of quasi-global precipitation from the wide variety of modern satellite-borne precipitation-related sensors. Estimates are provided at relatively fine scales ($0.25^\circ \times 0.25^\circ$, 3-h) in both real and post-real time to accommodate a wide range of researchers. However, the errors inherent in the finest scale estimates are large. The most successful use of the TMPA data is when the analysis takes advantage of the fine-scale data to create time/space averages appropriate to the user’s application (Huffman et al., 2010).

TMPA/3B42 is a quasi-global product (55 S 55 N) that combines microwave precipitation estimates from various satellite microwave radiometers:

- TMI on TRMM spacecrafts
- SSM/I (on DMSP satellites)
- AMSU B on NOAA satellite series
- AMSR E on Aqua satellite

It “imposes” quality of TRMM TMI on other sensors. TMPA Is being followed up by IMERG (Integrated Multi-satellitE Retrievals for Global Precipitation Mission).

3B42RT_Daily.20160509.7

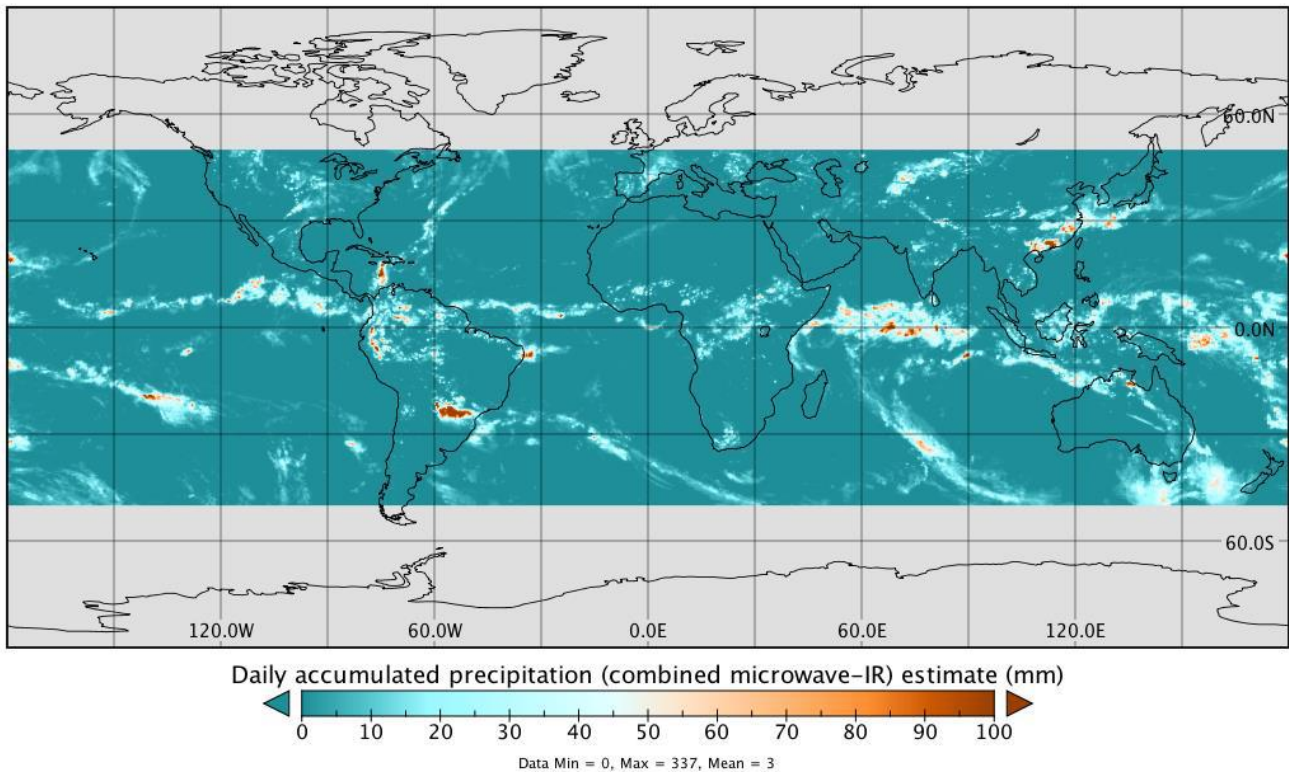


Figure 20. Daily Accumulated Precipitation (combined microwave-IR) estimate (mm), TMPA

CMORPH (CPC MORPHing technique) produces global precipitation analyses at high spatial and temporal resolution. This technique uses precipitation estimates that have been derived from low orbiter satellite microwave observations *exclusively*, and whose features are transported via spatial propagation information that is obtained entirely from geostationary satellite IR data. Precipitation estimates derived from the passive microwaves aboard the DMSP 13, 14 & 15 (SSM/I), the NOAA-15, 16, 17 & 18 (AMSU-B), and AMSR-E and TMI aboard NASA's Aqua and TRMM spacecraft have been incorporated. These estimates are generated by algorithms of Ferraro (1997) for SSM/I, Ferraro et al. (2000) for AMSU-B and Kummerow et al. (2001) for TMI. This technique is not a precipitation estimation algorithm but a means by which estimates from existing microwave rainfall algorithms can be combined. Therefore, this method is extremely flexible such that any precipitation estimates from any microwave satellite source can be incorporated.

With regard to spatial resolution, although the precipitation estimates are available on a grid with a spacing of 8 km (at the equator), the resolution of the individual satellite-derived estimates is coarser than that - more on the order of 12 x 15 km or so. The finer "resolution" is obtained via interpolation.

In effect, IR data are used as a means to transport the microwave-derived precipitation features during periods when microwave data are not available at a location. Propagation vector matrices are produced by computing spatial lag correlations on successive images of geostationary satellite IR which are then used to propagate the microwave derived precipitation estimates. This process governs the movement of the precipitation features only. At a given location, the shape and intensity of the precipitation features in the intervening half hour periods between microwave scans are determined by performing a time-weighting interpolation between microwave-derived features that

have been propagated forward in time from the previous microwave observation and those that have been propagated backward in time from the following microwave scan (Joyce et al., 2004).

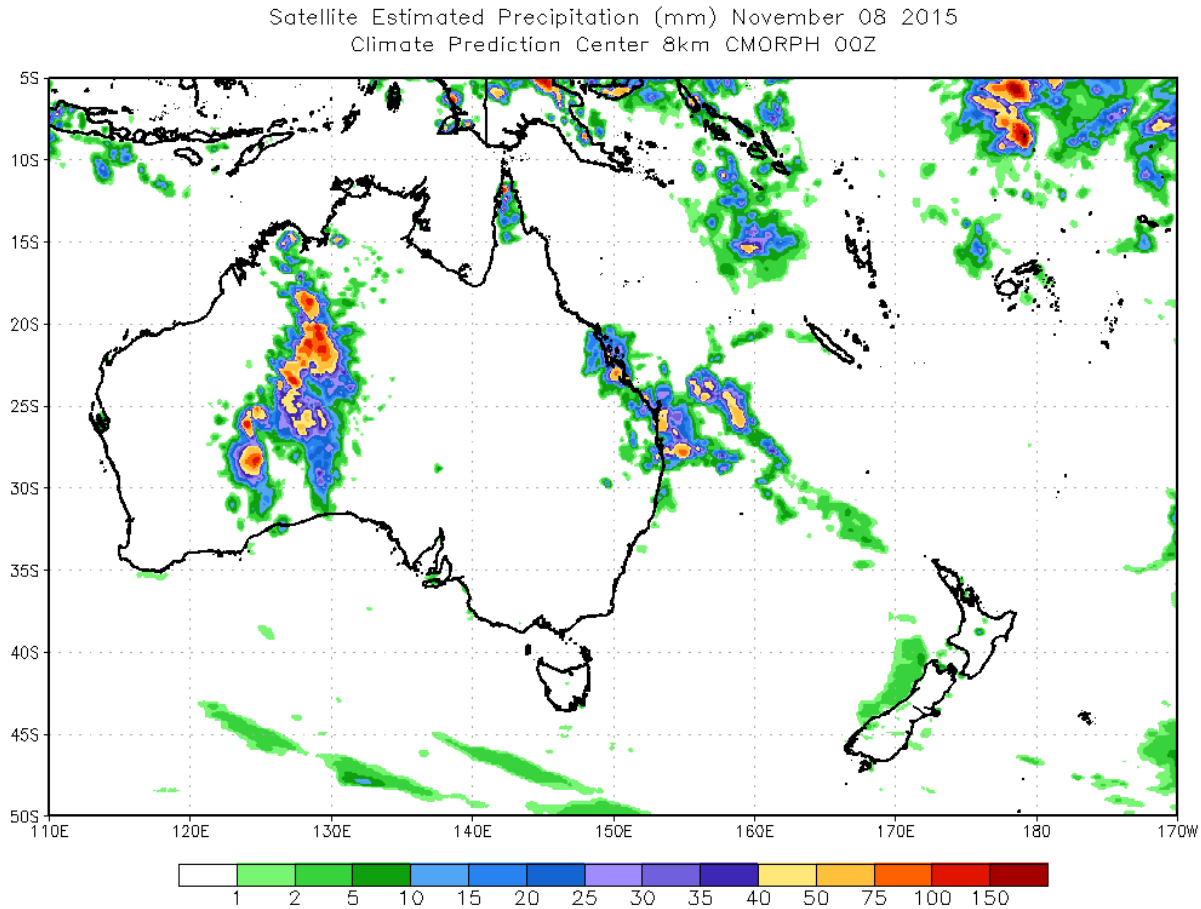


Figure 21. Satellite Estimated Precipitation (mm), CMORPH

2.4.5 Climatic Research Unit (CRU) Global Land Precipitation Data

The Climate Research Unit (CRU) dataset has been constructed at the University of East Anglia. This dataset provides monthly global precipitation at $0.5^\circ \times 0.5^\circ$ spatial resolution from 1900 to the present. The data is available for public via the Centre of Environmental Data Archival (<https://crudata.uea.ac.uk/cru/data/hrg/>).

2.4.6 Global Precipitation Climatology Centre Monthly Product

The GPCP V2018 Full Data Monthly Product provides precipitation estimation at $0.5^\circ \times 0.5^\circ$ spatial resolution for the period from 1891 to the present. This dataset uses the data of rain gauges from 75,000 stations over the globe and includes extensive quality control and further weather dependent corrections. This data can be obtained through <https://www.esrl.noaa.gov/psd/data/gridded/data.gpcp.html> website.

2.4.7 PERSIANN-CDR

PERSIANN-CDR (Precipitation Estimation from Remotely Sensed Information using Artificial Neural Networks - Climate Data Record) developed by the Center for Hydrometeorology and Remote Sensing (CHRS) at the University of California, Irvine (UCI) provides daily rainfall estimates at 0.25° for the latitude band 60°N - 60°S over the period of 01/01/1983 to 12/31/2019 (and updated every quarter). PERSIANN-CDR is aimed at addressing the need for a consistent, long-term, high-resolution

and global precipitation dataset for studying the changes and trends in daily precipitation, especially extreme precipitation events, due to climate change and natural variability. PERSIANN-CDR is generated from the PERSIANN algorithm using GridSat-B1 infrared data and adjusted using the Global Precipitation Climatology Project (GPCP) monthly product to maintain consistency of the two datasets at 2.5 deg monthly scale throughout the entire record. The PERSIANN-CDR product is available to the public as an operational climate data record via the NOAA NCDC CDR Program website under the Atmospheric CDRs category.

<http://rainsphere.eng.uci.edu/>
www.ncdc.noaa.gov/cdr/operationalcdrs.html

2.4.8 Soil moisture to rainfall (SM2RAIN)

This method uses the water balance model to estimate precipitation from change in soil water storage (soil moisture).

$$P(t) = Z\Delta S(t) + E(t) + R(t) + g(t)$$

- ΔS = Change in storage
- P = Precipitation
- E = Evapotranspiration
- R = Runoff
- g = percolation

SM2RAIN-ASCAT is a new global scale rainfall product obtained from ASCAT satellite soil moisture data through the SM2RAIN algorithm (Brocca et al., 2014). The SM2RAIN-ASCAT rainfall dataset (in mm/day) is provided over an irregular grid at 12.5 km on a global scale. The product represents the cumulated rainfall between the 00:00 and the 23:59 UTC of the indicated day. The SM2RAIN method was applied to the ASCAT soil moisture product (Wagner et al., 2013) for the period from January 2007 to August 2019 (13 years).

The rainfall dataset is provided in netCDF format. A total of 12 netCDF files, one per year, are provided. The quality flag provided with the dataset has been used to mask out low quality data, as well as the areas characterised by complex topographic, frozen soil, and presence of tropical forests.

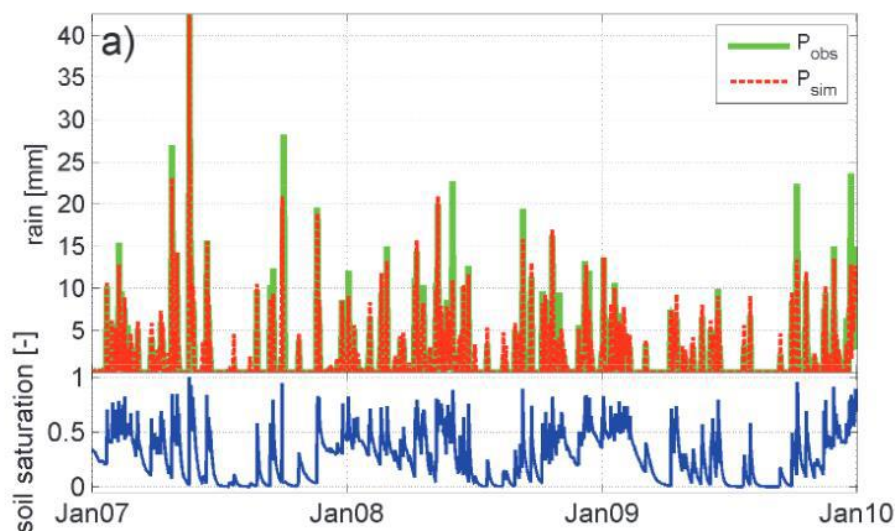


Figure 22. Estimating Rainfall from Satellite Soil Moisture Data

As we can see, there are a number of satellite precipitation products. The comparison of results obtained from different datasets shows that the daily mean precipitation is very close one to each other (Figure 23).

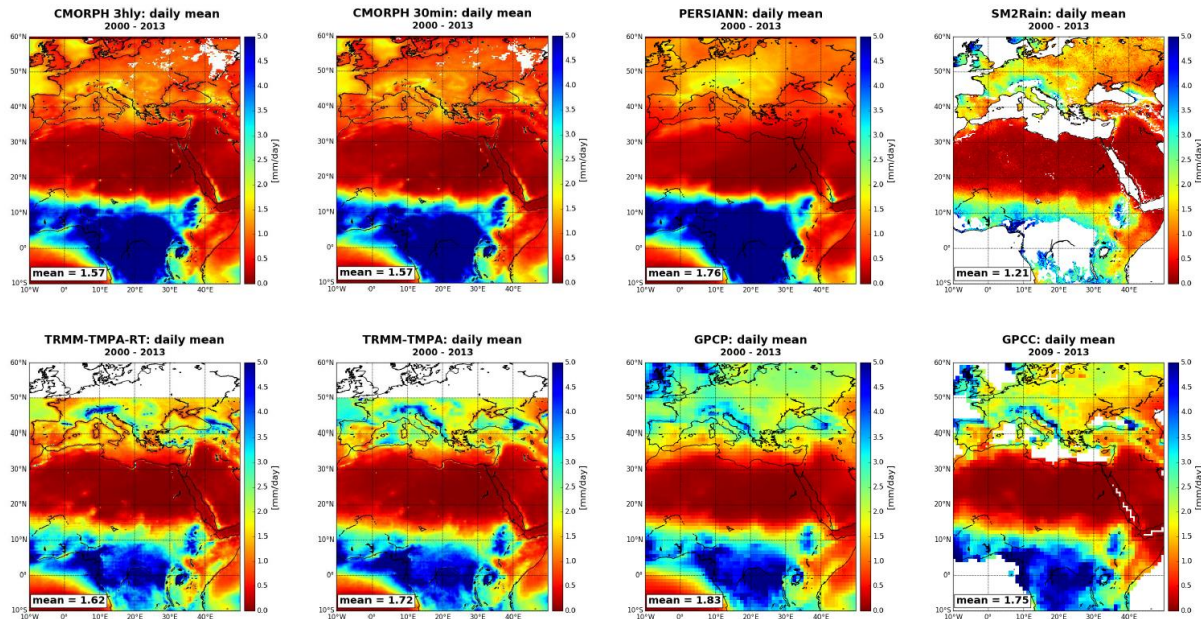


Figure 23. Daily Mean Temperature Calculated from the Different Satellite Products. Source: Technical University of Wien

However, when we compare the maximum 5-day precipitation amount (consecutive 5-day precipitation) precipitation, we can see that the results vary greatly (Figure 24).

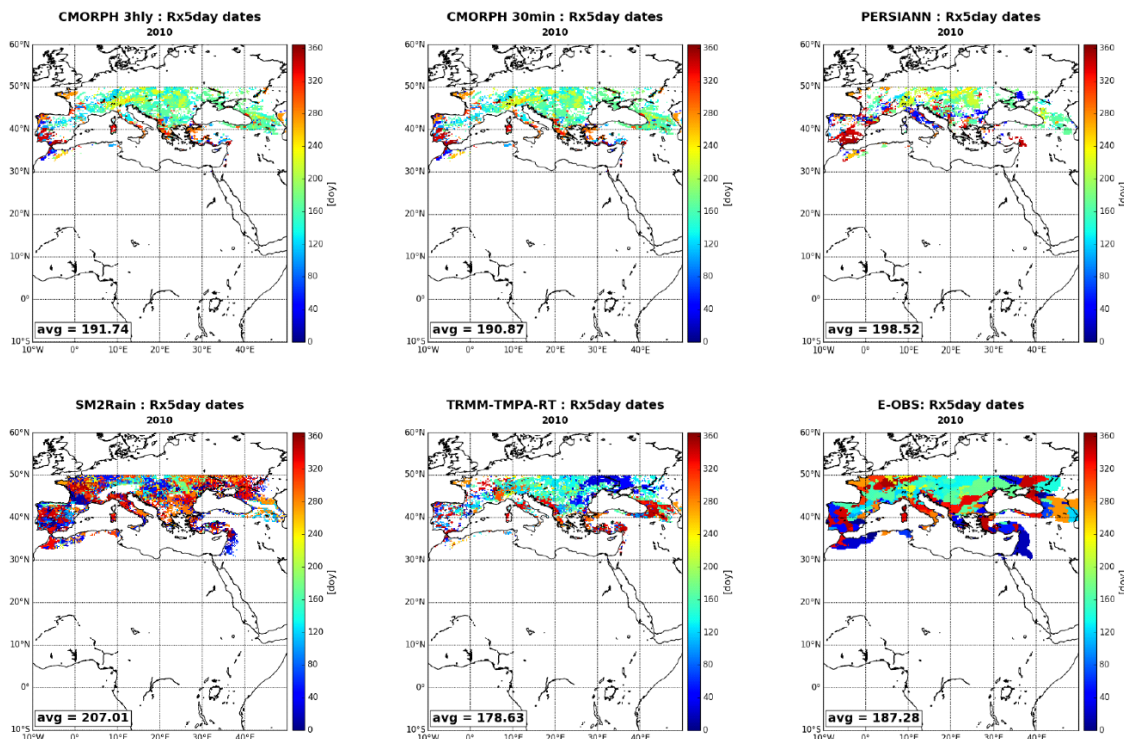


Figure 24. Maximum 5-day precipitation amount Calculated from the Different Satellite Products. Source: Technical University of Wien

Short-term precipitation data is especially important for the analysis and prediction of extremal hydrometeorological events (floods, mudflows, landslides, etc.).

Therefore, in order to select appropriate satellite imagery product for the specific territory, it is important to check and validate the image using the ground-based measurements.

2.4.9 Analysis of the precipitation datasets for Armenia based on international practices performed by Center for Hydrometeorology and Remote Sensing (CHRIS) at University of California Irvine

Analysis of two commonly used gridded Long-term (1900-2015) Datasets (GPCC V8 and CRU).

These two rainfall datasets have been processed and prepared to provide global coverage and both date back to the start date of 1900.

1. Figure 25 shows the spatial patterns of mean annual precipitation at 50km grid resolution, over Armenia for both GPCC V8 and CRU for the period of 1900-2015. Relatively speaking, both data sets show similar patterns for the Northern and upper parts of Western Armenia.
2. Figure 26 which is more relevant to this discussion shows the result of trend analysis for these two datasets. As can be seen, the long-term data shows **No detectable trend in precipitation over Armenia over the 115 years (1900-2015) analyzed by either dataset, suggesting that on the average over 115 years, there is no indication of any statistically detectable positive or negative trends in precipitation.**

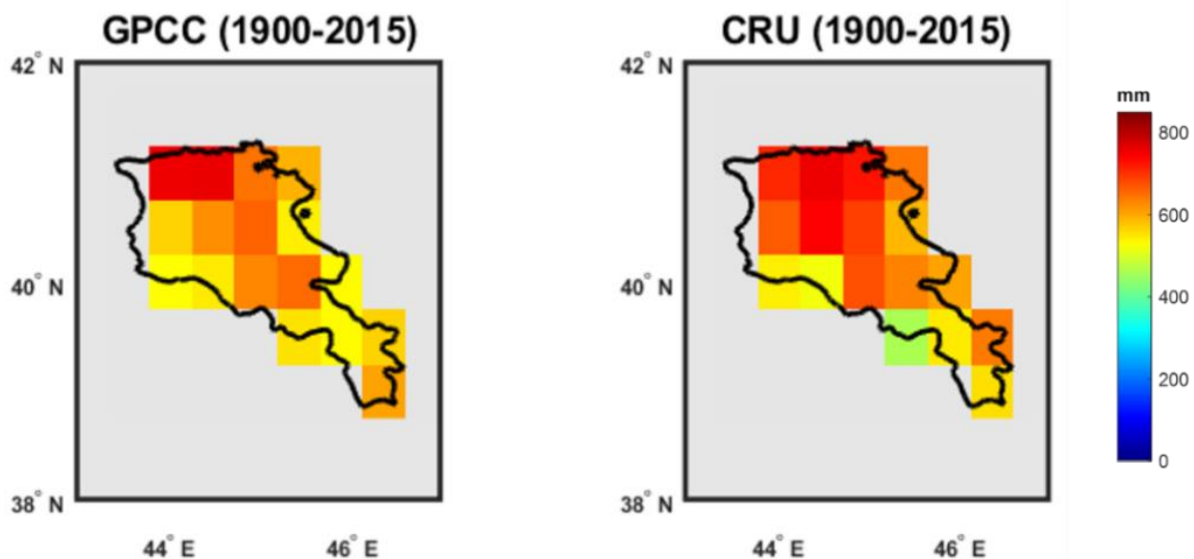


Figure 25. Spatial patterns of annual precipitation over Armenia for GPCC-V8 and CRU datasets

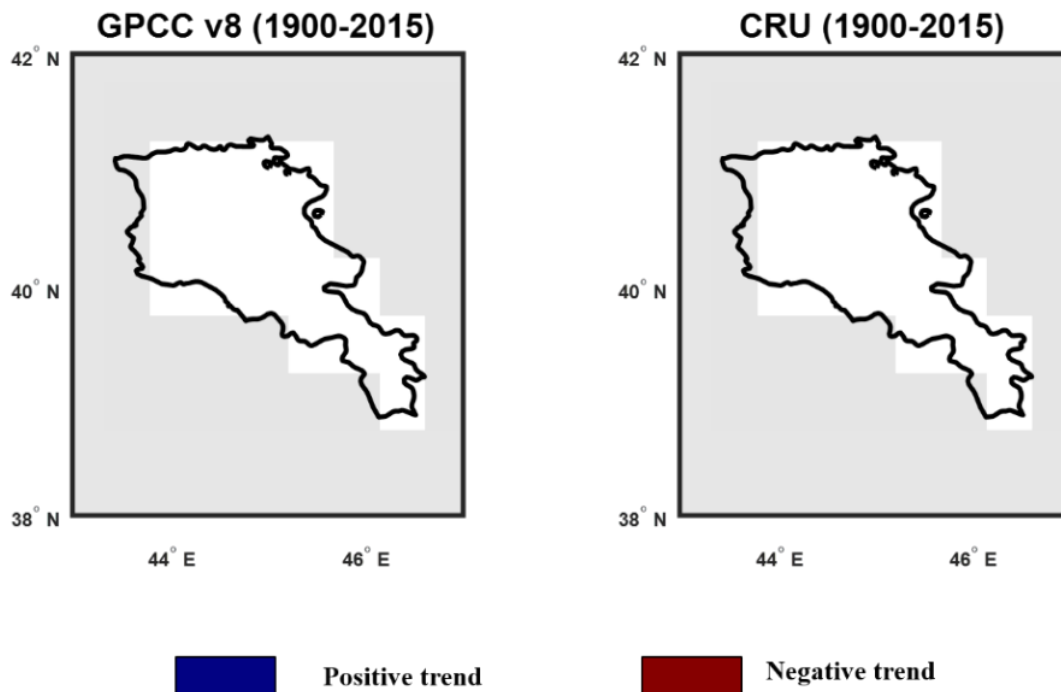


Figure 26. Long-term trends in precipitation over Armenia for GPCC-V8 and CRU datasets

Analysis of 3 datasets (GPCC-V8, CRU and PERSIANN-CDR) over the period of 1983-2015.

An additional high-resolution satellite-based dataset, the PERSIANN-CDR is available started from 1983.

Figure 27 shows the spatial patterns of mean annual precipitation for the three datasets over the period of (1983-2015). As can be seen, in general the three datasets agree with each other about the spatial patterns indicating that, on the average, the northern half of Armenia receiving more precipitation. Please note that PERSIANN-CDR having a finer resolution (25km) as compared to the other 2 (50km), provides more detailed observation with respect to spatial heterogeneity.

Figure 28 which again is more relevant to this discussion shows the result of trend analysis for the three datasets (GPCC-V8, CRU and PERSIANN-CDR). As can be seen, the over 3 decades of data show that:

- Both GPCC-V8 and PERSIANN-CDR show either no trend over some areas of Armenia and positive trend over some regions, especially the southern half of the country. Again, the PERSIANN-CDR because of its higher resolution provides much finer details.
- In this case CRU did not show any trend.

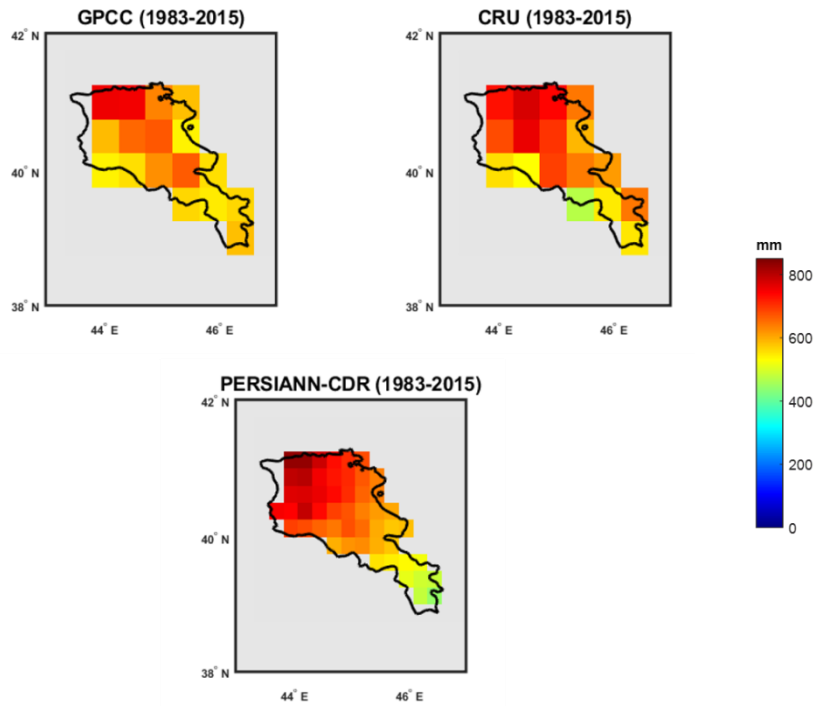


Figure 27. Spatial patterns of annual precipitation over Armenia for GPCC-V8 (50km), CRU (50km) and PERSIANN-CDR (25km) datasets over the period (1983-2015)

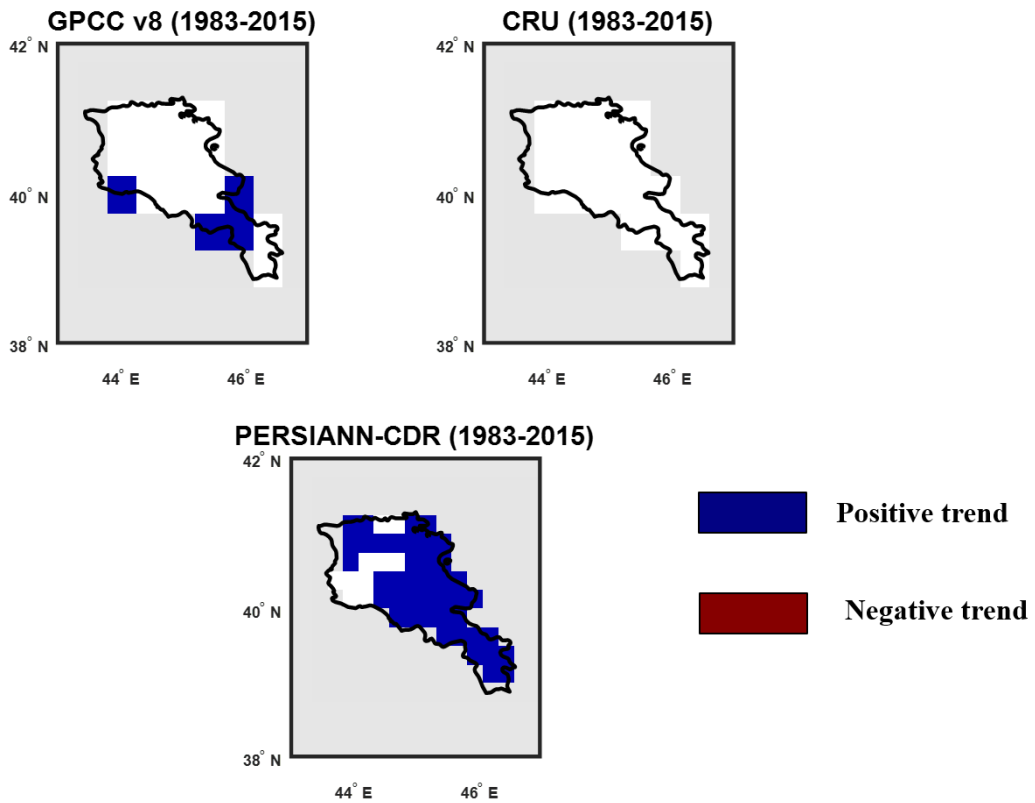


Figure 28. Precipitation trends over the three decades of study for the three datasets (GPCC-V8, CRU and PERSIANN-CDR) over Armenia for GPCC-V8 and CRU datasets.

2.4 Satellite Measurement of Evapotranspiration

Evapotranspiration is the sum of evaporation from the land surface plus transpiration from plants.

Evapotranspiration (E) is defined as actual evapotranspiration (E_a)—the actual rate at which water vapor is returned to the atmosphere from the ground and by plants and potential evapotranspiration (E_p)—the water vapor flux under ideal conditions of complete ground cover by plants, uniform plant height and leaf coverage, and an adequate water supply (Miller, 2007).

There are several projects that estimate global evapotranspiration using satellite remote sensing data.

2.4.1 Global Land Evaporation Amsterdam Model (GLEAM)

GLEAM (Global Land Evaporation Amsterdam Model) is a set of algorithms that separately estimate the different components of land evaporation (or 'evapotranspiration'): transpiration, bare-soil evaporation, interception loss, open-water evaporation and sublimation. Additionally, GLEAM provides surface and root-zone soil moisture, potential evaporation and evaporative stress conditions.

The rationale of the method is to maximize the recovery of information on evaporation contained in current satellite observations of climatic and environmental variables. The Priestley and Taylor equation used in GLEAM calculates potential evaporation based on observations of surface net radiation and near-surface air temperature. Estimates of potential evaporation for the land fractions of bare soil, tall canopy and short canopy are converted into actual evaporation using a multiplicative evaporative stress factor based on observations of microwave Vegetation Optical Depth (VOD) and estimates of root-zone soil moisture. The latter is calculated using a multi-layer running-water balance. To try to correct for random forcing errors, observations of surface soil moisture are also assimilated into the soil profile. Interception loss is calculated separately in GLEAM using a Gash analytical model. Finally, estimates of actual evaporation for water bodies and regions covered by ice and/or snow are obtained using an adaptation of the Priestley and Taylor equation.

The key features of GLEAM algorithm are:

- Consideration of soil constraint on evaporation.
- Detailed parameterization of forest interception.
- Extensive use of microwave observations, which is an asset under cloudy conditions (Martens et al., 2017, Miralles et al., 2011) (Figure 29).

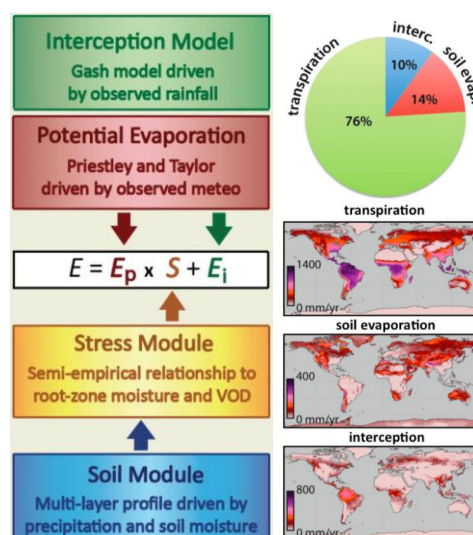


Figure 29. GLEAM Algorithm and Products

2.4.2 Global Land Data Assimilation System (GLDAS)

GLDAS is a global-scale terrestrial modeling system that integrates multisource information of the land surface and atmosphere with advanced land surface models and data assimilation techniques, aiming to model the optimal fields of land surface states and fluxes (Rodell et al., 2004). GLDAS v2.0 drives four land surface models³.

The goal of the Global Land Data Assimilation System (GLDAS) is to ingest satellite- and ground-based observational data products, using advanced land surface modeling and data assimilation techniques, in order to generate optimal fields of land surface states and fluxes (Rodell et al., 2004a). The software, which has been streamlined and parallelized by the Land Information System (LIS) sister project, drives multiple, offline (not coupled to the atmosphere) land surface models, integrates a huge quantity of observation-based data, executes globally at high resolutions (2.5-degrees to 1 km), and is capable of producing results in near-real time (Figure 30).

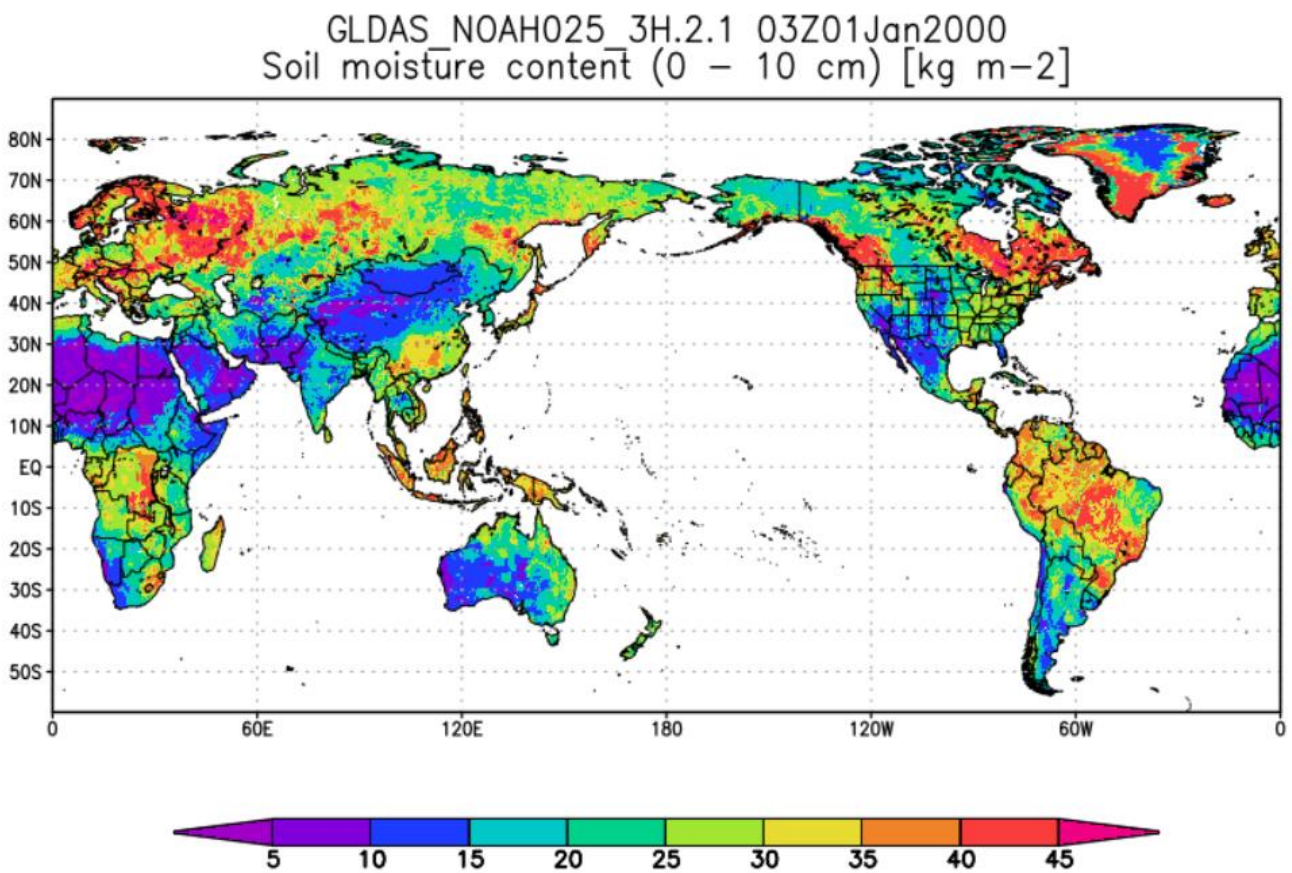


Figure 30. GLDAS_NOAH025_3H: GLDAS Noah Land Surface Model L4 3 hourly 0.25 x 0.25 degree V2.1

³ Document for NASA GLDAS Version 2 data products. 2018. The document can be download from: https://hydro1.gesdisc.eosdis.nasa.gov/data/GLDAS/GLDAS_CLSM025D.2.0/doc/README_GLDAS2.pdf

2.4.3 MODIS Global Evapotranspiration Project (MOD16)

This project is part of NASA/EOS project to estimate global terrestrial evapotranspiration from earth land surface by using satellite remote sensing data. MOD16 global evapotranspiration product can be used to calculate regional water and energy balance, soil water status; hence, it provides key information for water resource management. With long-term ET data, the effects of changes in climate, land use, and ecosystems disturbances (e.g. wildfires and insect outbreaks) on regional water resources and land surface energy change can be quantified.

The MOD16 global evapotranspiration (ET)/latent heat flux (LE)/potential ET (PET)/potential LE (PLE) datasets are regular 1-km² land surface ET datasets for the 109.03 Million km² global vegetated land areas at 8-day, monthly and annual intervals. The dataset covers the time period from 2000 to present (Figure 31).

The MOD16 ET datasets are estimated using Mu et al.s improved ET algorithm (2011) over previous Mu et al.s paper (2007a). The ET algorithm is based on the Penman-Monteith equation (Monteith, 1965). Surface resistance is an effective resistance to evaporation from land surface and transpiration from the plant canopy.

Terrestrial ET includes evaporation from wet and moist soil, from rain water intercepted by the canopy before it reaches the ground, and the transpiration through stomata on plant leaves and stems. Evaporation of water intercepted by the canopy is a very important water flux for ecosystems with a high LAI. Canopy conductance for plant transpiration is calculated by using LAI to scale stomatal conductance up to canopy level. For many plant species during growing seasons, stomatal conductance is controlled by vapor pressure deficit (VPD) (Oren et al., 1999; Mu et al., 2007b; Running Kimball, 2005) and daily minimum air temperature (Tmin). Tmin is used to control dormant and active growing seasons for evergreen biomes. High temperatures are often accompanied by high VPDs, leading to partial or complete closure of stomata. For a given biome type, two threshold values for Tmin and VPD are listed in the Biome-Property-Look-Up-Table (BPLUT) to control stomatal conductance (Mu et al., 2007a; 2009; 2011).

MOD16 products includes 8-day, monthly and annual ET, LE, PET, PLE and 8-day, annual quality control (ET_QC). The 8-day MOD16A2 QC field is inherited from MOD15A2 in the same period.

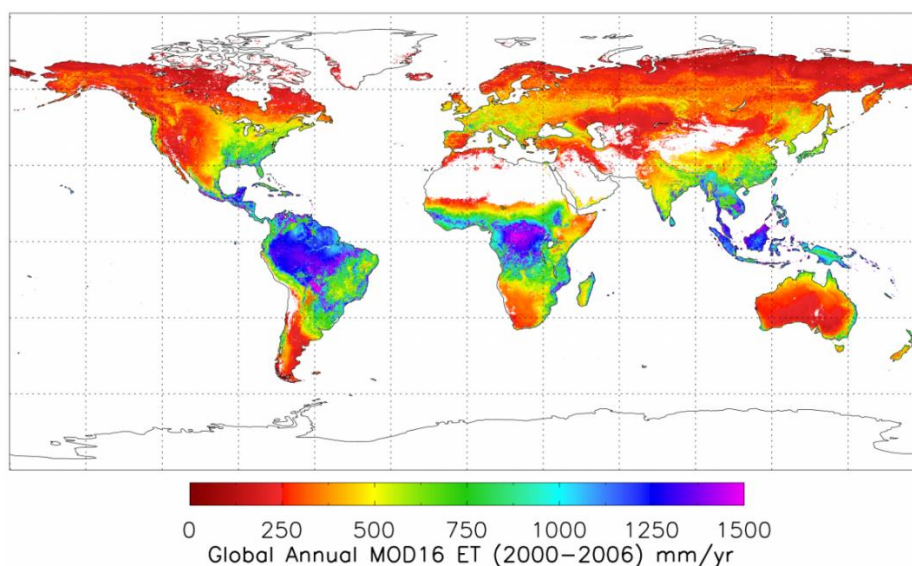


Figure 31. Global Annual Evapotranspiration (2000-2006) mm/yr, MOD16 Dataset

2.5 Land Surface Temperature (LST)

The Land Surface Temperature (LST) is the radiative skin temperature of the land surface, as measured in the direction of the remote sensor. It is estimated from Top-of-Atmosphere brightness temperatures from the infrared spectral channels of a constellation of geostationary satellites (Meteosat Second Generation, GOES, MTSAT/Himawari). Its estimation further depends on the albedo, the vegetation cover and the soil moisture.

LST is a mixture of vegetation and bare soil temperatures. Because both respond rapidly to changes in incoming solar radiation due to cloud cover and aerosol load modifications and diurnal variation of illumination, the LST displays quick variations too. In turn, the LST influences the partition of energy between ground and vegetation, and determines the surface air temperature.

Land surface temperature (LST) is a key parameter for climate change and land cover analysis and for many fields of study, for example, in agriculture, or in the estimation of several variables of environmental interest such as evapotranspiration. The computation of LST from satellite imagery is possible due to the advances in thermal infrared technology and its implementation in artificial satellites. For example, Landsat 8 incorporates Operational Land Imager (OLI) and Thermal InfraRed Sensor (TIRS) sensors the images from which, in combination with data from other satellite platforms (such as Terra and Aqua) provide all the information needed for the computation of LST. Different methodologies have been developed for the computation of LST from satellite images, such as single-channel and split-window methodologies.

The Global Land Service provides the following LST-based products:

- LST: hourly LST from instantaneous observations
- LST10-DC: 10-day Land Surface Temperature with Daily Cycle
- LST10-TCI: Thermal Condition Index with a 10-day composite of Land Surface Temperature.

2.5.1 MODIS Land Surface Temperature and Emissivity (MOD11)

The Land Surface Temperature (LST) is the radiative skin temperature of the land surface, as measured in the direction of the remote sensor. It is estimated from Top-of-Atmosphere brightness temperatures from the infrared spectral channels of a constellation of geostationary satellites (Meteosat Second Generation, GOES, MTSAT/Himawari). Its estimation further depends on the albedo, the vegetation cover and the soil moisture.

LST is a mixture of vegetation and bare soil temperatures. Because both respond rapidly to changes in incoming solar radiation due to cloud cover and aerosol load modifications and diurnal variation of illumination, the LST displays quick variations too. In turn, the LST influences the partition of energy between ground and vegetation, and determines the surface air temperature (Figure 32).

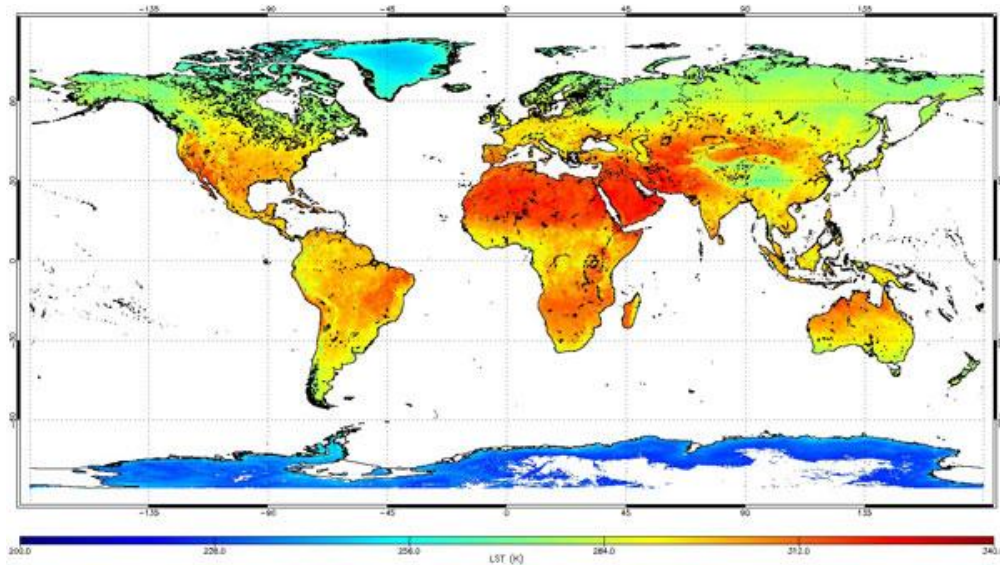


Figure 32. Land Surface Temperature composite for September 2016 of the Copernicus Sentinel-3 Satellite's SLSTR Instrument (Processed by D. Ghent, University of Southampton)

2.6 Land Use / Land Cover (LULC)

Land cover dataset can be obtained using different multi-spectral satellite images both free and commercial.

For instance, Sentinel-2 with 10-meter resolution and Landsat 7, 8 with 30-meter resolution are open source satellite products that can be used for land cover classification.

Proprietary products such as Rapid Eye with 5m resolution providing more accurate results but the cost of these images should be taken into account (\$1.9 for 1km²).

Flowchart of the land cover / land use classification using the Sentinel-2 imagery is presented below (Figure 33).

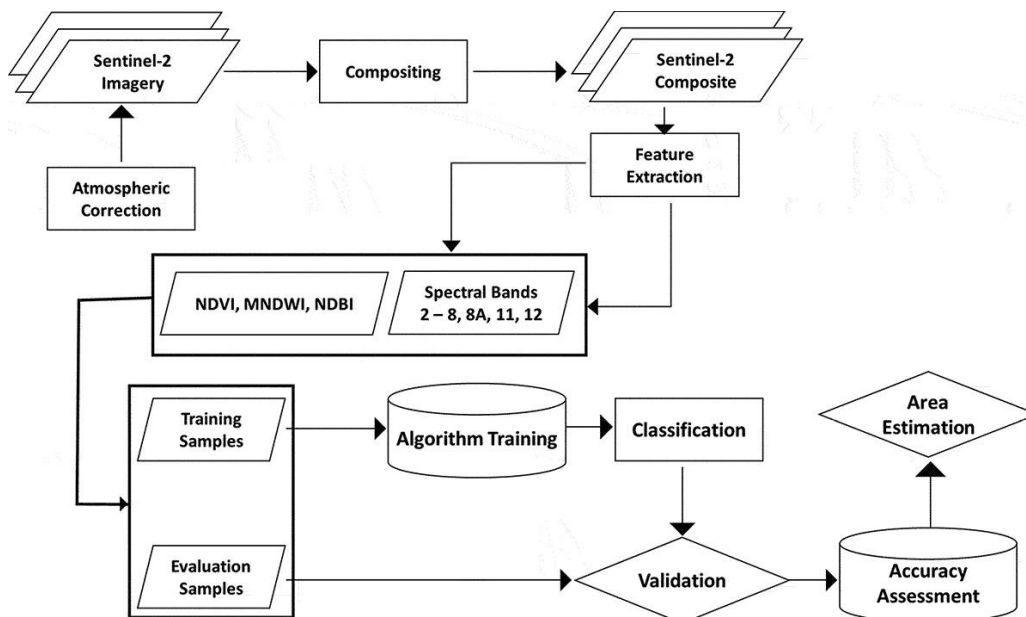


Figure 33. Land cover and land use classification performance of machine learning algorithms using Sentinel-2 data

In the frames of the USAID ASPIRED Project, the land cover / land use GIS layer and map has been developed for Ararat Valley (Figure 34). This layer has been integrated to the Decision Support System (DSS) developed by the project in order to be used in the water balance and other hydrological calculations.

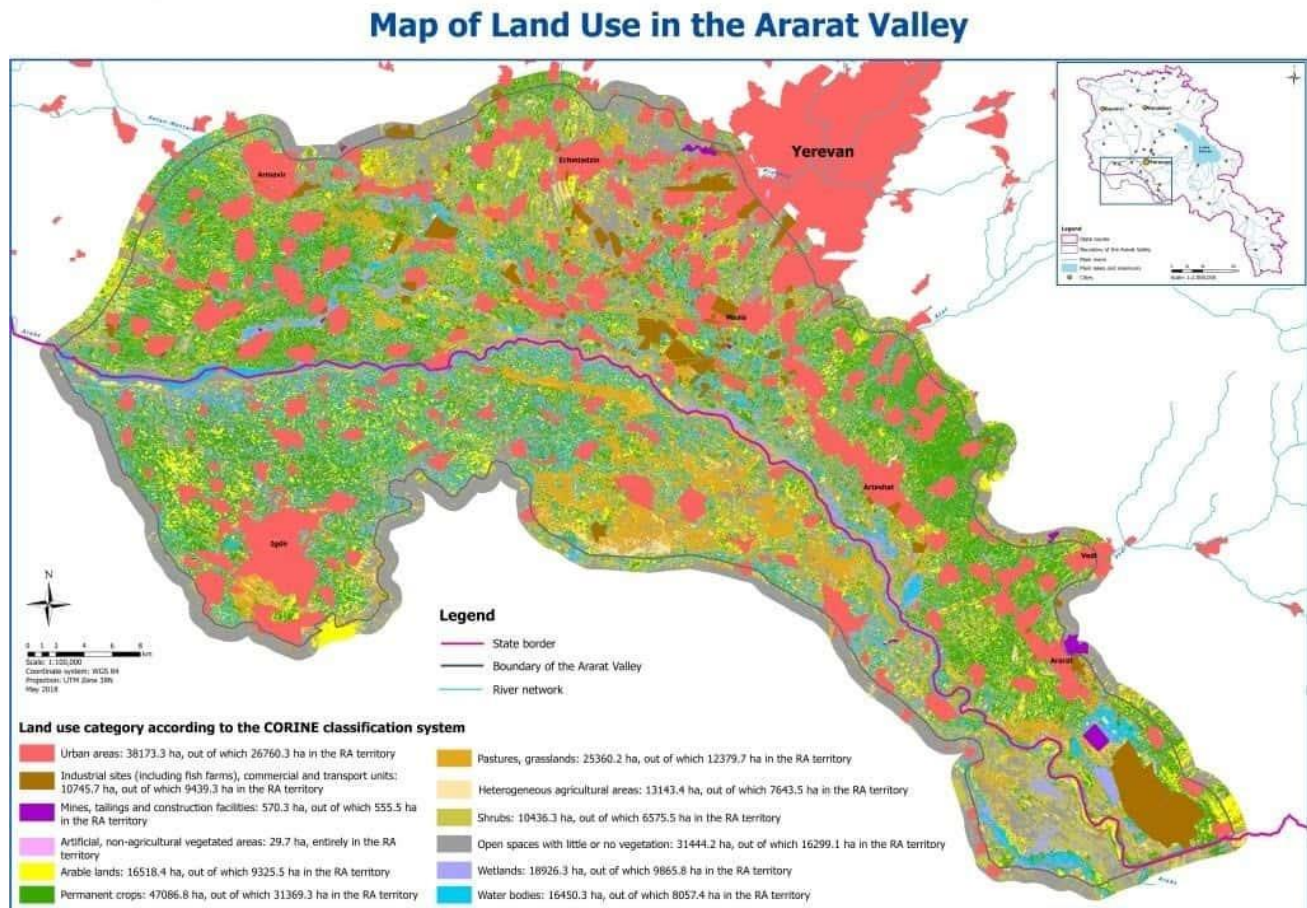


Figure 34. Land cover / Land Use Map of Ararat Valley⁴

2.7 Leaf Area Index (LAI)

The Leaf Area Index (LAI) of a plant canopy or ecosystem, defined as one half of the total green leaf area per unit horizontal ground surface area, measures the area of leaf material present in the specified environment. On sloping surfaces, the leaf area should be projected to the underlying ground along the normal to the slope. This dimensionless variable varies between 0 and values of about 10 or so, depending on local conditions. It partly controls important mass and energy exchange processes, such as radiation and rain interception, as well as photosynthesis and respiration, which couple vegetation to the climate system. Hence, LAI appears as a key variable in many models describing vegetation–atmosphere interactions, particularly with respect to the carbon and water cycles. LAI is recognized as an Essential Climate Variable (ECV) by the Global Climate Observing System (GCOS).

⁴ <https://www.meandahq.com/usaids-and-aspired-thanked-for-land-cover-and-land-use-classification-of-ararat-valley/>

LAI 300m product is being obtained through Sentinel-3/OLCI PROBA-V sensor since January, 2014.

- Daily LAI 300m is estimated by applying a Neural Network on
 - instantaneous Top-of-Canopy reflectances from Sentinel-3 OLCI (v1.1 products),
 - or daily Top-of-Aerosol input reflectances from PROBA-V (v1.0).
- Temporal smoothing and small gap filling is applied to the instantaneous LAI estimates, discriminating Evergreen Broadleaf Forest (EBF) and no-EBF pixels.
- Temporal compositing is adapted to provide a near-real time (10-daily) estimate and successive updated estimates until a consolidated value is reached after about 2 months.⁵

LAI 300m product is available through Copernicus Global Land Service (Figure 35).⁶

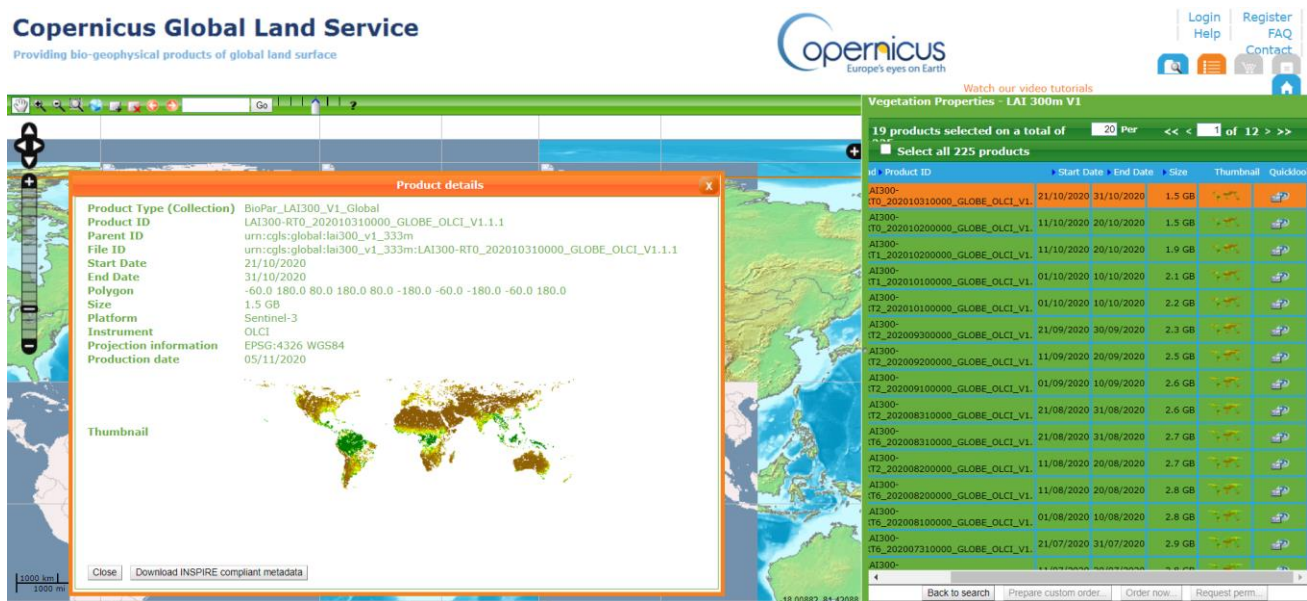


Figure 35. Leaf Area Index (LAI) Products in Coprnicus Global Land Service Portal

2.8 Elevation

One of the most important inputs for catchment hydrology is land surface elevation. Digital elevation models (DEM) are nowadays the most commonly used elevation data format. DEMs are typically derived from remote sensing data. The technologies of DEM generation are:

Photogrammetry

- Interferometric Radar
- Light Detection and Ranging (LiDAR)
- Flow directions are derived from DEM

There are 3 popular free Global DEM sources: SRTM, ASTER, and ALOS.

⁵ <https://land.copernicus.eu/global/products/lai>

⁶ <https://land.copernicus.vgt.vito.be/>

Space Shuttle Radar Topography Mission (SRTM)

The Shuttle Radar Topography Mission (SRTM) was flown aboard the space shuttle Endeavour February 11-22, 2000. The National Aeronautics and Space Administration (NASA) and the National Geospatial-Intelligence Agency (NGA) participated in an international project to acquire radar data which were used to create the first near-global set of land elevations.

The radars used during the SRTM mission were actually developed and flown on two Endeavour missions in 1994. The C-band Spaceborne Imaging Radar and the X-Band Synthetic Aperture Radar (X-SAR) hardware were used on board the space shuttle in April and October 1994 to gather data about Earth's environment. The technology was modified for the SRTM mission to collect interferometric radar, which compared two radar images or signals taken at slightly different angles. This mission used single-pass interferometry, which acquired two signals at the same time by using two different radar antennas. An antenna located on board the space shuttle collected one data set and the other data set was collected by an antenna located at the end of a 60-meter mast that extended from the shuttle. Differences between the two signals allowed for the calculation of surface elevation.

Endeavour orbited Earth 16 times each day during the 11-day mission, completing 176 orbits. SRTM successfully collected radar data over 80% of the Earth's land surface between 60° north and 56° south latitude with data points posted every 1 arc-second (approximately 30 meters). SRTM DEM can be downloaded from <https://www2.jpl.nasa.gov/srtm/>.

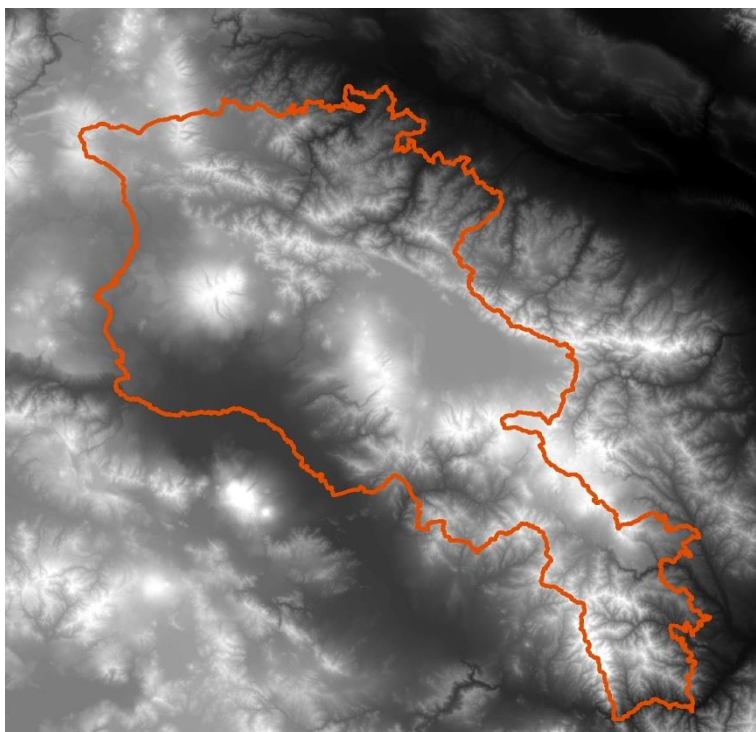


Figure 36. SRTM DEM with 1 arc-second Resolution for the Territory of Armenia

ASTER Global Digital Elevation Model (ASTER GDEM)

The Ministry of Economy, Trade, and Industry (METI) of Japan and the United States National Aeronautics and Space Administration (NASA) jointly announced the release of the Advanced

Spaceborne Thermal Emission and Reflection Radiometer (ASTER) Global Digital Elevation Model Version 3 (GDEM 003), and the ASTER Water Body Dataset (ASTWBD) on August 5, 2019.

The first version of the ASTER GDEM, released in June 2009, was generated using stereo-pair images collected by the ASTER instrument onboard Terra. ASTER GDEM coverage spans from 83 degrees north latitude to 83 degrees south, encompassing 99 percent of Earth's landmass.

The improved GDEM V3 adds additional stereo-pairs, improving coverage and reducing the occurrence of artifacts. The refined production algorithm provides improved spatial resolution, increased horizontal and vertical accuracy. The ASTER GDEM V3 maintains the GeoTIFF format and the same gridding and tile structure as V1 and V2, with 30-meter postings and 1 x 1 degree tiles.

An additional global product is now available: the ASTER Water Body Dataset (ASTWBD). This raster product identifies all water bodies as either ocean, river, or lake. Each GDEM tile has a corresponding Water Body tile.

The GDEM and ASTWBD are available for download from <https://earthdata.nasa.gov/>.

JAXA's Global ALOS 3D World ALOS DEM

ALOS World 3D is a 30-meter resolution digital surface model (DSM) captured by the Japan Aerospace Exploration Agency's (JAXA). Recently, this DSM has been made available to the public. The neat thing about it is that it is the most precise global-scale elevation data now. It uses the Advanced Land Observing Satellite "DAICHI" (ALOS) based on stereo mapping from PRISM.

ALOS World 3D DSM can be downloaded from https://www.eorc.jaxa.jp/en/distribution/standard_dataset/.

Next Steps

in the second report of National Expert on Water Resources Climate Risk and Vulnerability Assessment within this Assignment, the results of estimation of evapotranspiration for the entire territory of Armenia based on MOD16 dataset projection of evapotranspiration for 2040, 2070 and 2100 will be presented. Satellite data on evapotranspiration will be calibrated based on the actual measurements performed at key reference meteorological stations of Armenia.

Soil moisture change trends in Armenia will be analyzed as well. Soil moisture is a source of water for evapotranspiration over the continents, and is involved in both the water and the energy cycles. Soil moisture was recognized as an Essential Climate Variable (ECV) in 2010 and is fundamental for improving our understanding of long-term dynamics in the coupled water, energy, and carbon cycles over land. A range of long-term satellite-based soil moisture datasets are produced by Climate and Environmental Remote Sensing (CLIMERS) research group of the TU Wien⁷. These datasets will be used for our assessments.

⁷ <https://climers.geo.tuwien.ac.at/climers/>

Literature

1. Adger, W. 2006. "Vulnerability." *Global Env. Change* 16: 268-81.
2. Allan, R.P.; Liu, C.; Zahn, M.; Lavers, D.A.; Koukouvagias, E.; Bodas-Salcedo, A. Physically consistent responses of the global atmospheric hydrological cycle in models and observations. *Surv. Geophys.* 2014, 35, 533–552.
3. Allier, D., Vittecoq, B., and Mardhel, V. 2008. Assessment of the Intrinsic Vulnerability of Groundwater in Martinique. Bureau of Geological and Mining Research RP-56283-FR. (in French)
4. Benedict, I.; van Heerwaarden, C.C.; Weerts, A.H.; Hazeleger, W. The benefits of spatial resolution increase in global simulations of the hydrological cycle evaluated for the Rhine and Mississippi basins. *Hydrol. Earth Syst. Sci.* 2019, 23, 1779–1800.
5. Brocca, L., Filippucci, P., Hahn, S., Ciabatta, L., Massari, C., Camici, S., Schüller, L., Bojkov, B., and Wagner, W.: SM2RAIN–ASCAT (2007–2018): global daily satellite rainfall data from ASCAT soil moisture observations, *Earth Syst. Sci. Data*, 11, 1583–1601, <https://doi.org/10.5194/essd-11-1583-2019>, 2019.
6. Cleugh, H. A., R. Leuning, Q. Mu and S. W. Running (2007) Regional evaporation estimates from flux tower and MODIS satellite data. *Remote Sensing of Environment*, Volume 106, page 285–304 (doi: 10.1016/j.rse.2006.07.007)
7. Climate Change 2001: The Scientific Basis. Contribution of Working Group I to the Third Assessment Report of the Intergovernmental Panel on Climate Change (IPCC). Chapter: 13
8. Climate Change Analysis for the Ararat Valley, USAID ASPIRED Project, 2019.
9. Dirmeyer, P.A.; Schlosser, C.A.; Brubaker, K.L. Precipitation, recycling and land memory: An integrated analysis. *J. Hydrometeorol.* 2009, 10, 278–288.
10. Draft River Basin Management Plan for Hrazdan River Basin District in Armenia. EUWI+, Yerevan, 2020.
11. Draft River Basin Management Plan for Sevan River Basin District in Armenia. Part 1 – Characterization Phase. EUWI+, Yerevan, 2020.
12. Feng, G.-L.; Wu, Y.-P. Signal of acceleration and physical mechanism of water cycle in Xinjiang, China. *PLoS ONE* 2016, 11, 0167387.
13. GCOS. The Global Observing System for Climate: Implementation Needs; GCOS-200;WMO: Geneva, Switzerland, 2016; p. 315. Available online: <https://gcos.wmo.int/en/gcos-implementation-plan>
14. GIZ. 2014. The Vulnerability Sourcebook: Concept and Guidelines for Standardized Vulnerability Assessments. <https://www.adelphi.de/en/publications/list>.
15. Groisman, P.Y.; Knight, R.W.; Karl, T.R.; Easterling, D.R.; Sun, B.; Lawrimore, J.H. Contemporary changes of the hydrological cycle over the contiguous United States: Trends derived from in situ observations. *J. Hydrometeorol.* 2004, 5, 64–85.
16. Harding, R.; Best, M.; Blyth, E.; Hagemann, S.; Kabat, P.; Tallaksen, L.M.; Warnaars, T.; Wiberg, D.; Weedon, G.P.; van Lanen, H.; et al. WATCH: Current knowledge of the terrestrial global water cycle. *J. Hydrometeorol.* 2011, 12, 1149–1156.
17. Haverd, V.; Raupach, M.R.; Briggs, P.R.; Canadell, J.G.; Isaac, P.; Pickett-Heaps, C.; Roxburgh, S.H.; van Gorsel, E.; Viscarra Rossel, R.A.; Wang, Z. Multiple observation types reduce uncertainty in Australia's terrestrial carbon and water cycles. *Biogeosciences* 2013, 10, 2011–2040.

18. Held, I.M.; Soden, B.J. Robust responses of the hydrological cycle to global warming. *J. Clim.* 2006, 19, 5686–5699.
19. Hinkel, J. 2011. "Indicators of Vulnerability and Adaptive Capacity: Towards a Clarification of the Science-Policy Interface." *Global Env. Change* 21 (1): 198-208.
20. Huffman G.J., Adler R.F., Bolvin D.T., Nelkin E.J. (2010) The TRMM Multi-Satellite Precipitation Analysis (TMPA). In: Gebremichael M., Hossain F. (eds) *Satellite Rainfall Applications for Surface Hydrology*. Springer, Dordrecht. https://doi.org/10.1007/978-90-481-2915-7_1
21. Idé K. S., Niandou, S. A., Naimi, M., Chikhaoui M., in Schimmel, K. (2019): Analysis of water resources vulnerability assessment tools. *Journal of Agricultural Science and Technology*, B 9, str. 69–86. DOI: 10.17265/2161-6264/2019.02.001
22. IPCC, 2007: *Climate Change 2007: The Physical Science Basis. Contribution of Working Group I to the Fourth Assessment Report of the Intergovernmental Panel on Climate Change* [Solomon, S., D. Qin, M. Manning, Z. Chen, M. Marquis, K.B. Averyt, M.Tignor and H.L. Miller (eds.)]. Cambridge University Press, Cambridge, United Kingdom and New York, NY, USA.
23. IPCC, 2014: *Climate Change 2014: Synthesis Report. Contribution of Working Groups I, II and III to the Fifth Assessment Report of the Intergovernmental Panel on Climate Change* (Core Writing Team, R.K. Pachauri and L.A. Meyer (eds.)). IPCC, Geneva, Switzerland, 151 pp.
24. J. A. A. Jones. *Global Hydrology: Processes, Resources and Environmental Management*. Longman, 1997
25. Joyce, R. J., J. E. Janowiak, P. A. Arkin, and P. Xie, 2004: CMORPH: A method that produces global precipitation estimates from passive microwave and infrared data at high spatial and temporal resolution. *J. Hydromet.*, 5, 487-503.
26. Jung, M., M. Reichstein, P. Ciais, S.I. Seneviratne, J. Sheffield, M. L. Goulden, G. B. Bonan, A. Cescatti, J. Chen, R. de Jeu, A. J. Dolman, W. Eugster, D. Gerten, D. Gianelle, N. Gobron, J. Heinke, J. S. Kimball, B. E. Law, L. Montagnani, Q. Mu, B. Mueller, K. W. Oleson, D. Papale, A. D. Richardson, O. Roupsard, S. W. Running, E. Tomelleri, N. Viovy, U. Weber, C. Williams, E. Wood, S. Zaehle and K. Zhang (2010_ Recent decline in the global land evapotranspiration trend due to limited moisture supply. *Nature*, Volume 467, page 951--954 - October 2010 (doi: 10.1038/nature09396)
27. Lahoz, W.; Khatatov, B.; Ménard, R. *Data Assimilation—Making Sense of Observations*; Springer: Dordrecht, The Netherlands, 2010; p. 302; ISBN 978-3-540-74702-4.
28. Levizzani, V.; Cattani, E. *Satellite Remote Sensing of Precipitation and the Terrestrial Water Cycle in a Changing Climate*. *Remote Sens.* 2019, 11, 2301.
29. Margulis, S.A.; Wood, E.F.; Troch, P.A. The terrestrial water cycle: Modeling and data assimilation across catchment scales. *J. Hydrometeorol.* 2006, 7, 309–311.
30. Marin, M., Clinciu, I., Tudose, C., Ungurean, C., Adorjani, A., Mihalache A.L., Davidescu, A.A., Davidescu, S.O., Dinca, L., Cacovean, H. (2020) Assessing the vulnerability of water resources in the context of climate changes in a small forested watershed using SWAT: A review. *Environmental Research*, Volume 184, 2020, 109330, ISSN 0013-9351, <https://doi.org/10.1016/j.envres.2020.109330>.
31. Martens, B., Miralles, D.G., Lievens, H., van der Schalie, R., de Jeu, R.A.M., Fernández-Prieto, D., Beck, H.E., Dorigo, W.A., and Verhoest, N.E.C.: GLEAM v3: satellite-based land evaporation and root-zone soil moisture, *Geoscientific Model Development*, 10, 1903–1925, doi: 10.5194/gmd-10-1903-2017, 2017.

32. Martin, G.M. Quantifying and reducing uncertainty in the large-scale response of the water cycle. *Surv. Geophys.* 2014, 35, 553–575.
33. Miralles, D.G., Holmes, T.R.H., de Jeu, R.A.M., Gash, J.H., Meesters, A.G.C.A., Dolman, A.J.: Global land-surface evaporation estimated from satellite-based observations, *Hydrology and Earth System Sciences*, 15, 453–469, doi: 10.5194/hess-15-453-2011, 2011.
34. Montenegro, A., M. Eby, Q. Mu, M. Mulligan, A. J. Weaver, E. C. Wiebe, M. Zhao (2009) The net carbon drawdown of small-scale afforestation from satellite observations. *Global and Planetary Change* 69, page 195-204 (doi:10.1016/j.gloplacha.2009.08.005)
35. Mu, Q., F. A. Heinsch, M. Zhao, S. W. Running (2007) Development of a global evapotranspiration algorithm based on MODIS and global meteorology data. *Remote Sensing of Environment*, Volume 111, page 519-536 (doi: 10.1016/j.rse.2007.04.015)
36. Mu, Q., F.A. Heinsch, M. Zhao, S.W. Running (2007) MODIS global evapotranspiration (ET) products by Mu et al.
37. Mu, Q., L. A. Jones, J. S. Kimball, K. C. McDonald and S. W. Running (2009) Satellite assessment of land surface evapotranspiration for the pan-Arctic domain. *Water Resources Research*, Volume 45, Number W09420 - 2009 (doi: 10.1029/2008WR007189)
38. Mu, Q., M. Zhao, F. A. Heinsch, M. Liu, H. Tian and S. W. Running (2007) Evaluating water stress controls on primary production in biogeochemical and remote sensing-based models. *Journal of Geophysical Research*, Volume 112, Number G01012 (doi: 10.1029/2006JG000179)
39. Mu, Q., M. Zhao, J. S. Kimball, N. G. McDowell, S. W. Running (2013) A Remotely Sensed Global Terrestrial Drought Severity Index. *Bulletin of the American Meteorological Society*, 01/2013, Volume 94, Issue 1, Number 1, p.83.98, DOI:10.1175/BAMS-D-11-00213.1
40. Mu, Q., M. Zhao, S. W. Running (2011_ Improvements to a MODIS Global Terrestrial Evapotranspiration Algorithm *Remote Sensing of Environment*, Volume 115, pages 1781-1800 (doi:10.1016/j.rse.2011.02.019)
41. Nogueira, M. The sensitivity of the atmospheric branch of the global water cycle to temperature fluctuations at synoptic to decadal time-scales in different satellite- and model-based products. *Clim. Dyn.* 2019, 52, 617–636.
42. OECD. 2008. Handbook on Constructing Composite Indicators: Methodology and User Guide. <http://www.oecd.org/els/soc/handbookonconstructingcompositeindicatorsmethodologyanduserguide.htm>.
43. Rodell, M., 2004. Basin scale estimates of evapotranspiration using GRACE and other observations. *Geophys. Res. Lett.* 31 (20), L20504. <https://doi.org/10.1029/>
44. Rodell, M.; Houser, P.R.; Jambor, U.; Gottschalck, J.; Mitchell, K.; Meng, C.-J.; Arsenault, K.; Cosgrove, B.; Radakovich, J.; Bosilovich, M.; et al. The Global Land Data Assimilation System. *Bull. Am. Meteorol. Soc.* 2004, 85, 381–394.
45. Schneider, U.; Finger, P.; Meyer-Christofer, A.; Rustemeier, E.; Ziese, M.; Becker, A. Evaluating the hydrological cycle over land using the newly-corrected precipitation climatology from the Global Precipitation Climatology Centre (GPCC). *Atmosphere* 2017, 8, 52.
46. Sherwood, S.; Fu, Q. A drier future? *Science* 2014, 343, 737–739.
47. Shivhare, N., Prabhat Kumar Singh Dikshit, Shyam Bihari Dwivedi (2018) A Comparison of SWAT Model Calibration Techniques for Hydrological Modeling in the Ganga River Watershed, *Engineering*, Volume 4, Issue 5, 2018, Pages 643-652, ISSN 2095-8099, <https://doi.org/10.1016/j.eng.2018.08.012>.

48. Sinan, M., Maslouhi, R., and Razack, M. 2003. "Use of GIS for the Characterization of Vulnerability and Sensitivity to Groundwater Pollution." Presented at the 2nd FIG Regional Conference, Marrakech, Morocco, December 2-5, 2003. (in French)
49. Skliris, N.; Zika, J.D.; Nurser, G.; Josey, S.A.; Marsh, R. Global water cycle amplifying at less than the Clausius-Clapeyron rate. *Sci. Rep.* 2016, 6, 38752.
50. Sorooshian, S.; Hsu, K.-L.; Coppola, E.; Tomassetti, B.; Verdecchia, M.; Visconti, G. (Eds.) *Hydrological Modelling and the Water Cycle*; Springer: Dordrecht, The Netherlands, 2008; p. 302; ISBN 978-3642096648.
51. Tang, Q.; Oki, T. *Terrestrial Water Cycle and Climate Change—Natural and Human-Induced Impacts*; AGU-Wiley: Washington, DC, USA, 2016; 236p, ISBN 978-1-118-97176-5.
52. The Vulnerability Assessment of Water Resources of the Republic of Armenia under the Climate Change. "Development of Armenia's Fourth National Communication to the UNFCCC and Second Biennial Update Report" UNDP/GEF project, Yerevan, 2018.
53. Touch, T.; Oeurng, C.; Jiang, Y.; Mokhtar, A. Integrated Modeling of Water Supply and Demand Under Climate Change Impacts and Management Options in Tributary Basin of Tonle Sap Lake, Cambodia. *Water* 2020, 12, 2462.
54. Wang, X., Ma, F., and Li, J. 2012. "Water Resources Vulnerability Assessment Based on the Parametric-System Method: A Case Study of the Zhangjiakou Region of Guanting Reservoir Basin, North China." *Proced. Env. Sci.* 13 (3): 1204-12.
55. William Miller, III. *Trace Fossils: Concepts, Problems, Prospects*. Elsevier Science, 2007.
56. Wulfmeyer, V.; Turner, D.D.; Baker, B.; Banta, R.; Behrendt, A.; Bonin, T.; Brewer, W.A.; Buban, M.; Choukulkar, A.; Dumas, E.; et al. A new research approach for observing and characterizing land-atmosphere feedback. *Bull. Am. Meteorol. Soc.* 2018, 99, 1639–1667.
57. Yang, T.; Ding, J.; Liu, D.; Wang, X.; Wang, T. Combined use of multiple drought indices for global assessment of dry gets drier and wet gets wetter paradigm. *J. Clim.* 2019, 32, 737–748.
58. Zhang, K., J. S. Kimball, Q. Mu, L. A. Jones, S. Goetz and S. W. Running (2009) Satellite based analysis of northern ET trends and associated changes in the regional water balance from 1983 to 2005. *Journal of Hydrology*, Volume 379, page 92-110 - 2009 (doi: 10.1016/j.jhydrol.2009.09.047)